Neuron
Article

Activity Patterns Govern Synapse-Specific AMPA Receptor Trafficking between Deliverable and Synaptic Pools

Anders Kielland,[1,4,5] Genrieta Bochorishvili,[1,5] James Corson,[3] Lei Zhang,[1] Diane L. Rosin,[1] Paul Heggelund,[4] and J. Julius Zhu[1,2,*]
[1]Department of Pharmacology
[2]Department of Neuroscience
[3]Department of Psychology
University of Virginia, Charlottesville, VA 22908, USA
[4]Department of Physiology, Institute of Basic Medical Sciences, University of Oslo, Oslo, N-0317, Norway
[5]These authors contributed equally to this work
*Correspondence: jjzhu@virginia.edu
DOI 10.1016/j.neuron.2009.03.001

SUMMARY

In single neurons, glutamatergic synapses receiving distinct afferent inputs may contain AMPA receptors (-Rs) with unique subunit compositions. However, the cellular mechanisms by which differential receptor transport achieves this synaptic diversity remain poorly understood. In lateral geniculate neurons, we show that retinogeniculate and corticogeniculate synapses have distinct AMPA-R subunit compositions. Under basal conditions at both synapses, GluR1-containing AMPA-Rs are transported from an anatomically defined *reserve* pool to a *deliverable* pool near the postsynaptic density (PSD), but further incorporate into the PSD or functional *synaptic* pool only at retinogeniculate synapses. Vision-dependent activity, stimulation mimicking retinal input, or activation of CaMKII or Ras signaling regulated forward GluR1 trafficking from the *deliverable* pool to the *synaptic* pool at both synapses, whereas Rap2 signals reverse GluR1 transport at retinogeniculate synapses. These findings suggest that synapse-specific AMPA-R delivery involves constitutive and activity-regulated transport steps between morphological pools, a mechanism that may extend to the site-specific delivery of other membrane protein complexes.

INTRODUCTION

Native AMPA-Rs, assembled from homo- or heterotetrameric combinations of GluR1-4 subunits are the primary receptors mediating fast excitatory transmission in mammalian central synapses (Dingledine et al., 1999). AMPA-Rs with distinct subunit compositions exhibit different gating kinetics (Jonas, 2000; Mosbacher et al., 1994). Functionally distinct AMPA-Rs are not only expressed in different types of neurons but also at different synapses in the same neuron, which is essential for generating synaptic responses with very different time courses for processing different synaptic inputs (Gardner et al., 2001; Geiger et al., 1997; Rubio and Wenthold, 1997; Toth and McBain, 1998). However, how distinct AMPA-Rs are incorporated into different populations of synapses within the same neuron remains unknown. The same question can be generalized to the problem of how other proteins that are unevenly distributed or clustered in one or a few subcellular membrane compartments of the dendrite and/or axon travel to their destinations (e.g., Hoffman et al., 1997; Pelkey et al., 2006; Schaefer et al., 2007; Zhu, 2000). Previous studies of protein sorting and targeting in neurons and nonneuronal cells have suggested two general mechanisms (Lai and Jan, 2006; Mellman and Nelson, 2008; Schuck and Simons, 2004). The first scheme is preferential transportation and incorporation; many proteins are sorted into distinct transportation carriers, which deliver them into the membrane of appropriate cellular domains (i.e., axonal or apical and somatodendritic or basolateral domains [Burack et al., 2000; Matsuda et al., 2008; Sampo et al., 2003; Setou et al., 2000]). The second scheme is nonselective incorporation and preferential retention (including transcytosis); some proteins are incorporated into the membrane of both appropriate and inappropriate cellular domains but retained on the membrane surface only in the appropriate domain and preferentially endocytosed from the inappropriate domain (e.g., Casanova et al., 1990; Hammerton et al., 1991; Sampo et al., 2003; Setou et al., 2000; Yap et al., 2008). It is unclear which of these two mechanisms, or perhaps other yet uncharacterized schemes, is responsible for delivering distinct AMPA-Rs into different populations of synapses within the same neuron.

The lateral geniculate nucleus (LGN) is the primary thalamic relay that receives excitatory inputs from both the ascending retinal fibers and descending cortical fibers from layer 6 of the visual cortex (Sherman and Guillery, 2002; Steriade et al., 1997). Retinogeniculate (RG) synapses, although making up a small number of excitatory synapses (5%–10%), are powerful and effective in driving action potentials with precise timing to faithfully relay the visual information into the cortex

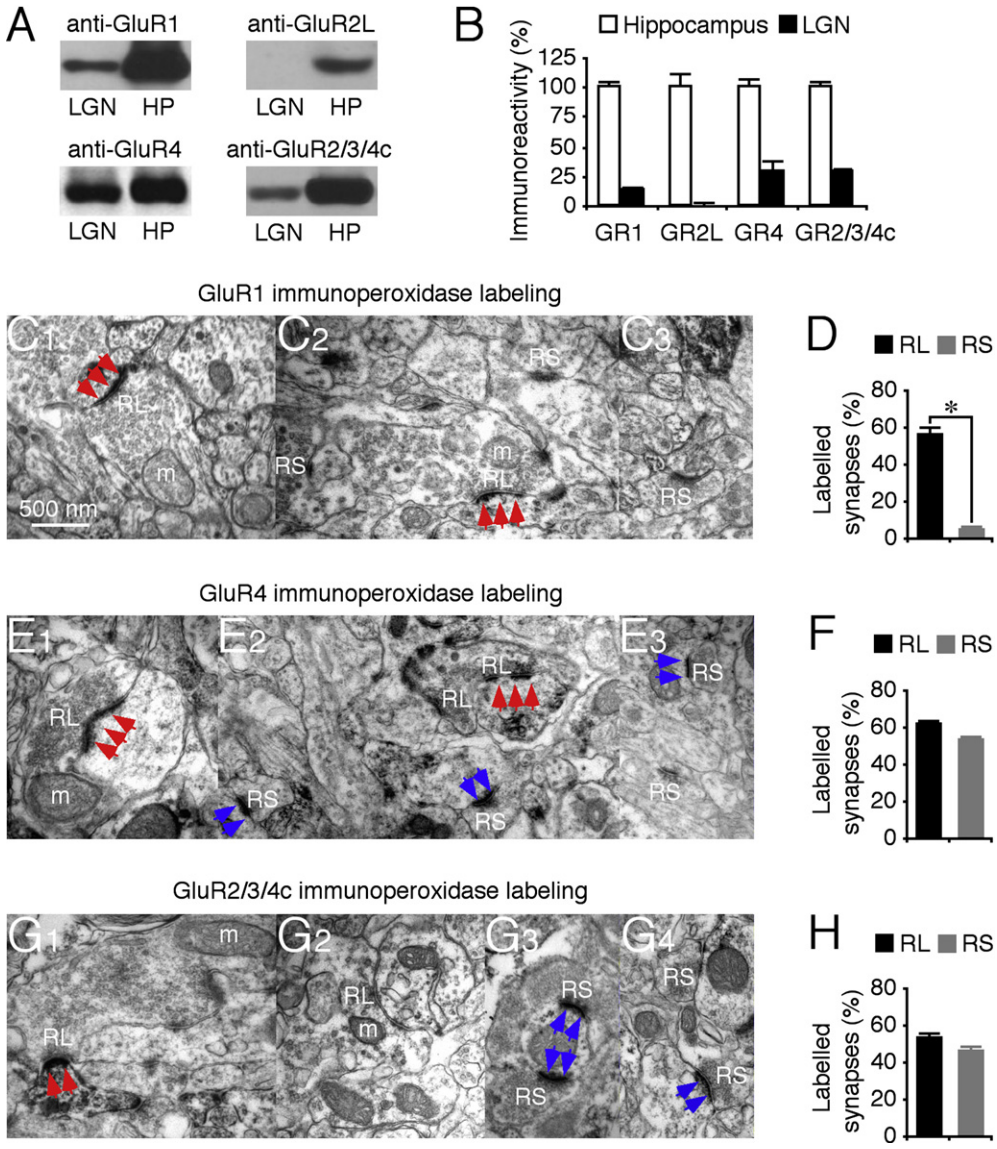

Figure 1. GluR1 Is Predominantly Expressed in Retinogeniculate Synapses

(A) Western blots of GluR1, GluR2L, GluR4, and GluR2/3/4c in the whole hippocampus (HP) and lateral geniculate nucleus (LGN) prepared from the same animals. Each pair of HP and LGN lanes was loaded with the same amount of protein (60–120 μg).

(B) Amounts of GluR1 (n = 8), GluR2L (n = 9), GluR4 (n = 8), and GluR2/3/4c (n = 8) in LGN relative to the whole hippocampus. The relative values and standard errors were normalized to average amounts of GluR1, GluR2L, GluR4, and GluR2/3/4c from whole hippocampus.

(C) GluR1 immunolabeling at synapses contacted by RL and RS terminals.

(D) Percentages of GluR1-labeled retinogeniculate (RG) and corticogeniculate (CG) synapses relative to all RG or CG synapses (n = 11; $p < 0.005$).

(E) GluR4 immunoperoxidase labeling at synapses contacted by RL and RS terminals.

(F) Percentages of GluR4-labeled RG and CG synapses relative to all RG or CG synapses (n = 15; $p = 0.09$).

(G) GluR2/3/4c immunoperoxidase labeling at synapses contacted by RL and RS terminals. Scale bar applies to (C1)–(G3). Arrows indicate positive immunoperoxidase labeling associated with PSD postsynaptic to RL (red) and RS (blue) terminals.

(H) Percentages of GluR2/3/4c-labeled RG and CG synapses relative to all RG or CG synapses (n = 10; $p = 0.06$). See Supplemental Data for the values.

(Augustinaite and Heggelund, 2007; Chen and Regehr, 2000; Liu and Chen, 2008; Usrey et al., 1998). Corticogeniculate (CG) synapses, on the other hand, constitute the majority of excitatory synapses on geniculate neurons, and they modulate retinogeniculate transmission. In particular, corticogeniculate inputs control the response mode, burst or tonic, of geniculate neurons by shafting postsynaptic membrane potential (Steriade et al., 1997; Wang et al., 2006). It is still unclear how the two types of excitatory synapses in LGN are capable of performing very different tasks and whether synapse-specific AMPA-R trafficking contributes to their diverse capabilities.

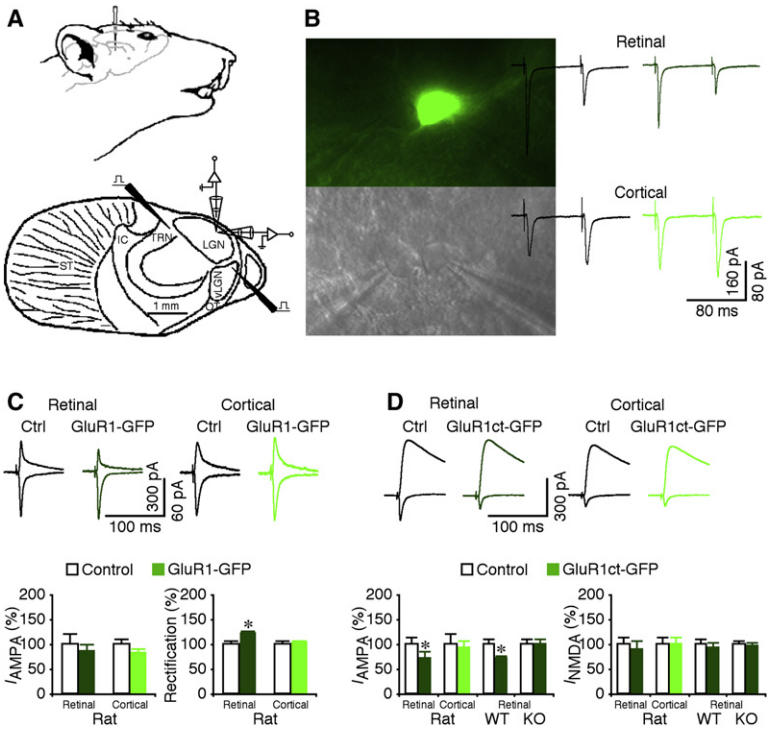

Figure 2. GluR1 Selectively Mediates Retinogeniculate Transmission

(A) Upper schematic drawing shows the setting for in vivo viral delivery of recombinant proteins into LGN. Lower schematic drawing illustrates the stimulating and recording electrode locations in the in vitro LGN preparation. IC, internal capsule; LGN, dorsal lateral geniculate nucleus; OT, optic tract; ST, striatum; TRN, thalamic reticular nucleus; vLGN, ventral lateral geniculate nucleus.

(B) Simultaneous recordings, made under transmitted light illumination (lower panel), from pairs of a recombinant protein-expressing neuron, identified by GFP fluorescence (upper panel), and a neighboring nonexpressing control neuron. Recording traces show AMPA-R-mediated EPSCs evoked by electrical stimulation of retinogeniculate (RG) and corticogeniculate (CG) afferents at −60 mV. Note the paired-pulse depression of RG responses and facilitation of CG responses of both control nonexpressing and expressing neurons.

(C) (Upper) Evoked AMPA-R-mediated responses at RG and CG synapses from nonexpressing (Ctrl) and GluR1-GFP-expressing neurons recorded at −60 mV and +40 mV. (Lower left) AMPA responses in neurons expressing GluR1-GFP at RG (n = 16; p = 0.55) and CG synapses (n = 20; p = 0.11) relative to neighboring control neurons. (Lower right) Rectification of GluR1-GFP-expressing neurons at RG (n = 16; $p < 0.005$) and CG synapses (n = 20; p = 0.88) relative to neighboring control cells. Rectification is defined as the ratio of responses at −60 mV and +40 mV.

(D) (Upper) Evoked AMPA-R- and NMDA-R-mediated responses at RG and CG synapses from nonexpressing (Ctrl) and GluR1ct-GFP-expressing neurons recorded at −60 mV and +40 mV. (Lower left) AMPA responses in GluR1ct-GFP-expressing neurons from rats at RG (n = 16; $p < 0.05$) and CG synapses (n = 15; p = 0.61), from wild-type (WT) mice (n = 24; $p < 0.005$), and from *GluR1* knockout (KO) mice (n = 24; p = 0.95) at RG synapses relative to neighboring control neurons. (Lower right) NMDA responses in GluR1ct-GFP-expressing neurons at RG (n = 16; p = 0.73) and CG synapses (n = 15; p = 0.87), from wild-type mice (n = 24; p = 0.75), and *GluR1* knockout mice (n = 24; p = 0.75) at RG synapses relative to neighboring control cells. Note that *GluR1* knockout mice had increased ratio of NMDA and AMPA responses compared to WT mice (n = 24; $p < 0.05$; Mann-Whitney Rank Sum test). AMPA-R- and NMDA-R-mediated current amplitude and standard errors were normalized to average values from control cells. Asterisks indicate statistical significance (Wilcoxon test). See Supplemental Data for the values.

In this study, we developed an experimental approach that combines an in vivo recombinant DNA delivery technique with an in vitro rodent LGN brain slice preparation (McCormack et al., 2006; Turner and Salt, 1998). The approach allows simultaneous examination of RG and CG synapses, which display distinct electrophysiological and ultrastructural properties (Steriade et al., 1997). Following molecular, sensory, and pharmacological manipulations in intact animals, we studied the impacts of the manipulations on nanoscale subcellular compartmental AMPA-R trafficking at RG and CG synapses, using electrophysiology and immunogold microscopy. We found that GluR1-containing AMPA-Rs were incorporated and mediated transmission only at proximately located RG synapses, not at distally located CG synapses. Surprisingly, immunoelectron microscopic images showed that GluR1 was present in the pools near the postsynaptic densities (PSDs) of both RG and CG synapses. Further investigation revealed that the vision-dependent activity pattern, present in the RG pathway but absent in the CG pathway, selectively drives forward trafficking of GluR1-containing AMPA-Rs into PSD of RG synapses to mediate transmission. These results reveal a scheme of nonselective transportation and preferential incorporation at locations where needed as a mechanism for destination-specific delivery of membrane proteins.

RESULTS

We first examined the AMPA-R composition in LGN. Western blots showed that LGN expressed GluR1, GluR4, and GluR2/3/4c, but not GluR2L (Figures 1A and 1B), consistent with previous reports (Kolleker et al., 2003; Martin et al., 1993; Mineff and Weinberg, 2000; Petralia and Wenthold, 1992). To determine the synaptic distribution of GluRs, we used immunoelectron microscopy. Retinal and cortical terminals are distinguishable at the ultrastructural level because of their characteristic appearance (Erisir et al., 1997; Kielland et al., 2006; Steriade et al., 1997). Retinal terminals have round vesicles, are large (RL terminals), contain pale mitochondria, and form asymmetric synapses with multiple release sites. Cortical terminals have round vesicles but are small (RS terminals), contain no or a few dark-appearing mitochondria, and form asymmetric synapses with single release sites. Immunoperoxidase labeling showed that GluR1 was primarily associated with synapses contacted by RL terminals, i.e., RG afferents, but only rarely (~4%) with synapses contacted by RS terminals, corresponding to CG (about two-thirds) and brainstem cholinergic (about one-third) afferents (Figures 1C and 1D). In contrast, immunoperoxidase labeling showed that GluR4 and GluR2/3/4c were equally associated with RG synapses and CG synapses (Figures 1E–1H).

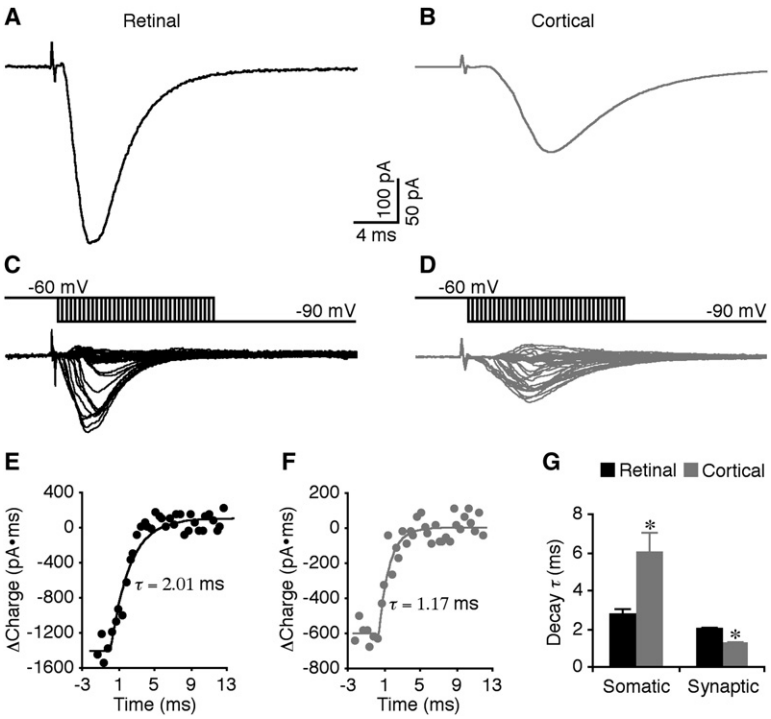

Figure 3. Time Courses of Evoked Retinogeniculate and Corticogeniculate Events at Synaptic Sites

(A and B) Evoked EPSCs in retinogeniculate (RG) and corticogeniculate (CG) pathways recorded at the soma of a thalamocortical neuron in LGN.

(C and D) Additional synaptic currents due to hyperpolarizing somatic voltage jumps made relative to EPSC onset (~–2 to –3 ms to 12–14 ms, 0.4 ms interval). Scale bars apply to (A)–(D).

(E and F) Charge recovery curves obtained from integration of voltage-jump-induced synaptic currents in (C) and (D).

(G) Decay time constant (τ) of evoked EPSCs in RG and CG pathways at somatic ($n = 11$; $p < 0.05$) and synaptic ($n = 11$; $p < 0.01$) sites. Asterisks indicate statistical significance Wilcoxon test). See Supplemental Data for the values.

GluR1 Selectively Mediates RG Transmission

To determine whether GluR1 primarily mediates RG transmission, we virally delivered GFP-tagged GluR1, GluR1-GFP, in rat LGN by in vivo microinjection (Figure 2A). This GluR1-GFP is a rectified or electrophysiologically "tagged" channel, and synaptic delivery of this receptor enhances rectification of transmission (Hayashi et al., 2000; Zhu et al., 2002). After ~15 hr of expression, we prepared LGN slices and made simultaneous recordings of evoked excitatory postsynaptic currents (EPSCs) of neuron pairs including a GluR-GFP-expressing neuron, identified by GFP fluorescence, and a nearby nonexpressing control neuron (Figure 2B). RG and CG EPSCs were evoked by independently stimulating the anatomically segregated RG and CG pathways using two stimulating electrodes, and they exhibited hallmark paired-pulse depression and facilitation, respectively, which served as a confirmation (Turner and Salt, 1998) (Figures 2A and 2B). Compared to nearby nonexpressing neurons, GluR1-GFP-expressing neurons had enhanced rectification of AMPA responses from RG synapses, but not from CG synapses (Figure 2C), indicating selective GluR1-GFP incorporation into RG synapses. Expression of GFP-tagged cytoplasmic termini of GluR1, GluR1ct-GFP, selectively blocks the trafficking of endogenous GluR1-containing AMPA-Rs (Kolleker et al., 2003; McCormack et al., 2006; Qin et al., 2005). GluR1ct-GFP-expressing neurons had depressed AMPA responses (by ~30%) from RG synapses, but not from CG synapses (Figure 2D). Expression of GluR1ct-GFP also depressed RG transmission (by ~30%) in LGN prepared from wild-type but not *GluR1* knockout mice (Figure 2D). Together, these results indicate that GluR1 selectively mediates RG transmission. As controls, using similar approaches (i.e., viral expression of GluR4-GFP, GluR2(R→Q)-GFP, GluR4ct-GFP, or GluR2ct-GFP), we found that GluR4-GFP- and GluR2-GFP-expressing neurons had enhanced rectification of AMPA responses from both RG and CG synapses and that GluR4ct-GFP and GluR2ct-GFP had depressed AMPA responses from both CG and RG synapses (Figure S1 available online). These results suggest that GluR4 and GluR2 mediate both CG and RG transmission, consistent with the immunoperoxidase labeling results (Figures 1E–1H).

The predominant synapse-specific involvement of GluR1, which has slower gating kinetics than other GluR subunits (Jonas, 2000), appears at odds with the fact that the evoked RG EPSCs have a faster time course compared to the evoked CG EPSCs (Figures 3A and 3B). However, this may reflect severe dendritic filtering and distortion of the EPSCs from CG synapses, which are more distally located than RG synapses (Steriade et al., 1997). Indeed, measuring the "true" decay time constant of synaptic events, using a voltage-jump technique (Hausser and Roth, 1997; Walker et al., 2002), revealed that at synaptic sites the decay time constant of CG EPSCs was ~40% faster than that of RG EPSCs (Figures 3C–3G), supporting the notion that RG synapses are enriched with the slow-gating AMPA-R subunit GluR1.

Ras Signals GluR1 Trafficking from Deliverable into Synaptic Pools

To examine how GluR1 is selectively delivered to mediate RG transmission, we quantified the GluR1 distribution in and near geniculate synapses using pre-embedding immunogold labeling (Figure 4). Surprisingly, GluR1 silver-gold particles were abundant at both RG and CG synapses (Figures 4A, 4D, and 4E). A significant proportion (~12%) of GluR1 silver-gold particles were located in PSD of RG synapses, whereas only a background amount (~1%) of GluR1 silver-gold particles were observed in PSD of CG synapses, consistent with a selective involvement of GluR1 in RG transmission. Interestingly, many GluR1 silver-gold particles (~18%) were located near PSD (~30–100 nm from the postsynaptic membrane) of both RG and CG synapses, in the cytosol or on the plasma membrane, forming a seemingly distinct AMPA-R pool. Small GTPase Ras and calcium/calmodulin-dependent protein kinase II (CaMKII) activities drive synaptic delivery of GluR1 (Hayashi et al., 2000; Zhu et al., 2002). In vivo viral expression of a constitutively active Ras, Ras(ca)-GFP, or a constitutively active CaMKII, CaMKII-IRES-GFP, increased the amount

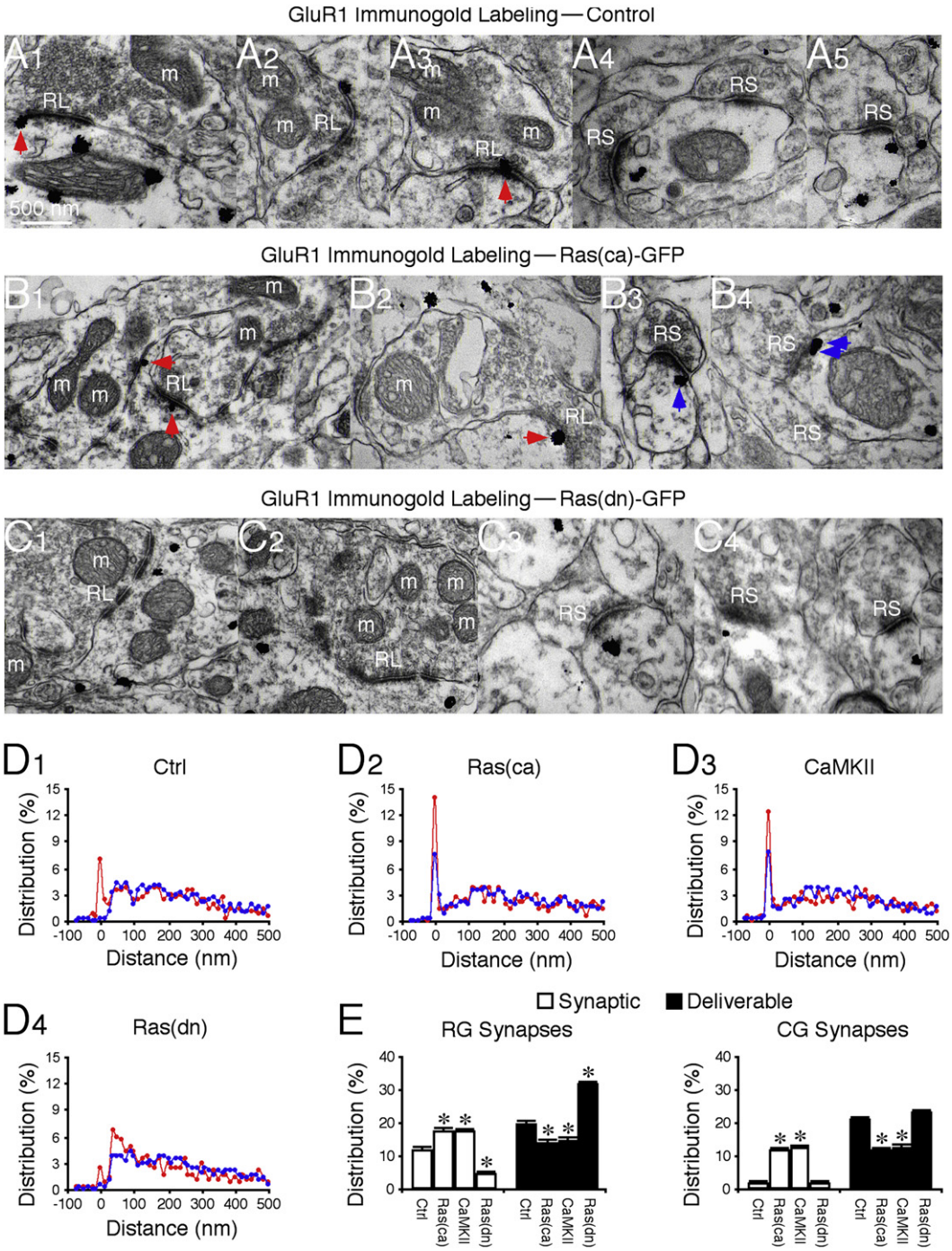

Figure 4. Ras Controls Forward GluR1 Trafficking from Deliverable to Synaptic Pools

(A–C) GluR1 immunogold labeling at synapses in normal control LGN (A1-5), LGN-expressing Ras(ca)-GFP (B1-4), and LGN-expressing Ras(dn)-GFP (C1-4). Arrows point to silver-enhanced gold particles associated with PSDs postsynaptic to RL (red arrows) or RS (blue arrows) terminals. Scale bar applies to (A)–(C).

(D) Relative distributions of GluR1 at synapses contacted by RL (red) and RS (blue) terminals in normal LGN (D1: n = 710 for RL; n = 1572 for RS), LGN-expressing Ras(ca)-GFP (D2: n = 625 for RL; n = 1544 for RS), CaMKII-IRES-GFP (D3: n = 616 for RL; n = 1380 for RS), and Ras(dn)-GFP (D4; n = 594 for RL; n = 1549 for RS).

(E) (Left) Average percentages of GluR1 silver-gold particles in synaptic and deliverable pools at synapses contacted by RL terminals in normal LGN (n = 12), LGN-expressing Ras(ca)-GFP (n = 12, $p < 0.05$), CaMKII-IRES-GFP (n = 9, $p < 0.05$), or Ras(dn)-GFP (n = 10, $p < 0.001$). (Right) Average percentages of GluR1 silver-gold particles in synaptic and deliverable pools at synapses contacted by RS terminals in normal LGN (n = 12), LGN-expressing Ras(ca)-GFP (n = 12, $p < 0.001$), CaMKII-IRES-GFP (n = 9, $p < 0.001$), or Ras(dn)-GFP (n = 10, $p > 0.05$). Note (not shown) that average percentages of GluR1 silver-gold particles in the residual pool at synapses contacted by RL (n = 9–12; $p > 0.05$) and RS (n = 9–12; $p > 0.05$) terminals were the same as that in normal LGN. Asterisks indicate statistical significance relative to normal control LGN (Mann-Whitney Rank Sum test). See Supplemental Data for the values.

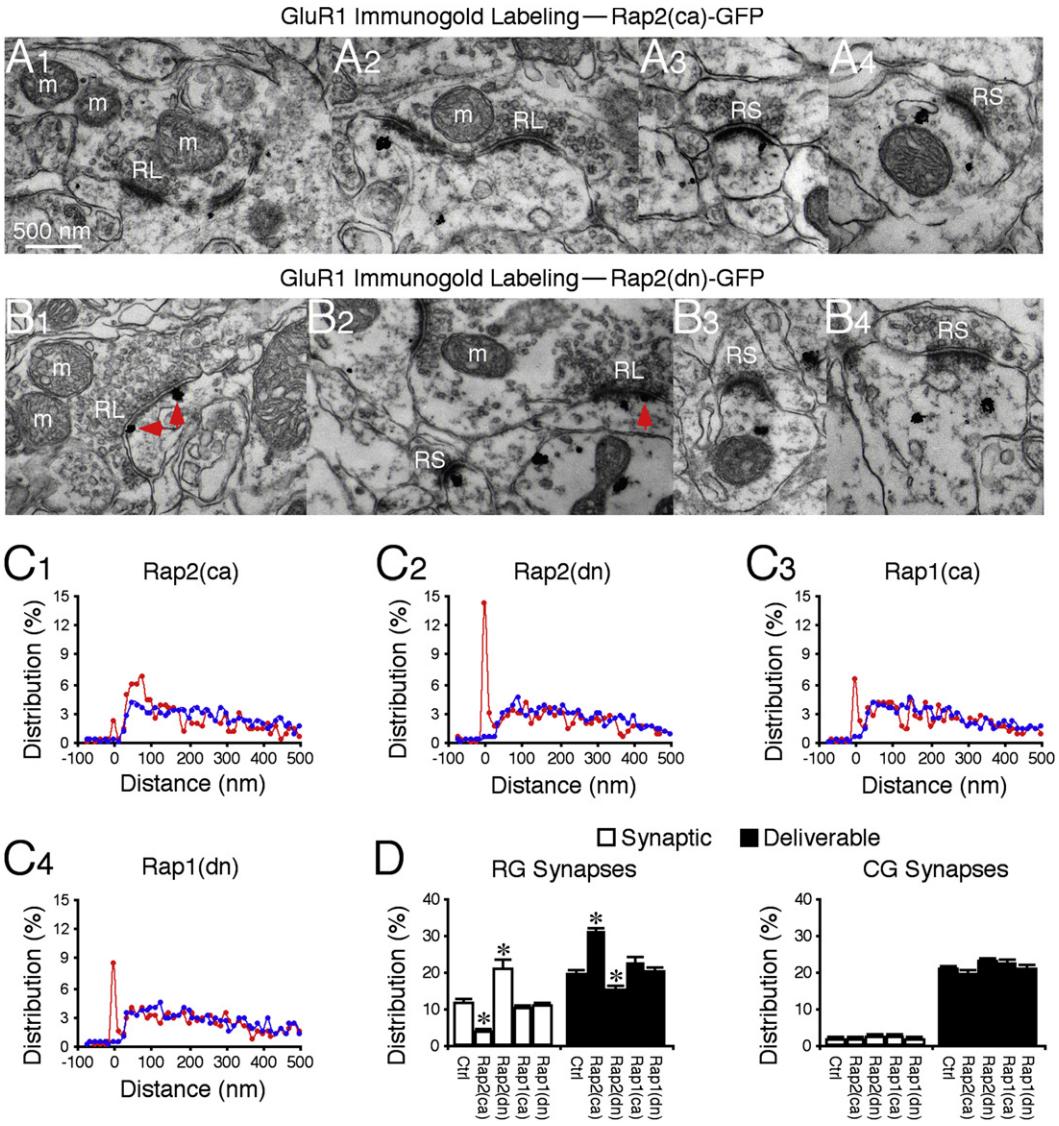

Figure 5. Rap2 Controls Reverse GluR1 Trafficking from Synaptic to Deliverable Pools

(A and B) GluR1 immunogold labeling at synapses in LGN-expressing Rap2(ca)-GFP (A1-4) and LGN-expressing Rap2(dn)-GFP (B1-4). Red arrows point to silver-enhanced gold particles associated with PSDs postsynaptic to RL terminals. Scale bar applies to (A) and (B).

(C) Relative distributions of GluR1 at synapses contacted by RL (red) and RS (blue) terminals in LGN-expressing Rap2(ca)-GFP (C1: n = 551 for RL; n = 1335 for RS), Rap2(dn)-GFP (C2: n = 462 for RL; n = 1243 for RS), Rap1(ca)-GFP (n = 534 for RL; n = 1238 for RS) and Rap1(dn)-GFP (n = 709 for RL; n = 1387 for RS).

(D) (Left) Average percentages of GluR1 silver-gold particles in synaptic and deliverable pools at synapses contacted by RL terminals in LGN-expressing Rap2(ca)-GFP (n = 10, $p < 0.001$), Rap2(dn)-GFP (n = 10, $p < 0.05$), Rap1(ca)-GFP (n = 10, $p > 0.05$), or Rap1(dn)-GFP (n = 10, $p > 0.05$) relative to normal control LGNs presented in Figure 2E. (Right) Average percentages of GluR1 silver-gold particles in synaptic and deliverable pools at synapses contacted by RS terminals in LGN-expressing Rap2(ca)-GFP (n = 10, $p > 0.05$), Rap2(dn)-GFP (n = 10, $p > 0.05$), Rap1(ca)-GFP (n = 10, $p > 0.05$), or Rap1(dn)-GFP (n = 10, $p > 0.05$) relative to normal control LGNs presented in Figure 2E. Note (not shown) that average percentages of GluR1 silver-gold particles in the residual pool at synapses contacted by RL (n = 10, $p > 0.05$) and RS (n = 10, $p > 0.05$) terminals were the same as that in normal LGN. Asterisks indicate statistical significance relative to normal control LGN (Mann-Whitney Rank Sum test). See Supplemental Data for the values.

of GluR1 silver-gold particles in PSD of RG synapses and reduced the number of GluR1 silver-gold particles by an equivalent amount in the nearby pool at these synapses (Figures 4B, 4D, and 4E). In contrast, expression of a dominant-negative form of Ras, Ras(dn)-GFP, which blocks endogenous Ras signaling (Zhu et al., 2002), reduced GluR1 in PSD and increased GluR1 by a corresponding number in the nearby pool at RG synapses (Figures 4C, 4D, and 4E). These results suggest that the AMPA-R pool near PSD represents a functionally distinct "deliverable" pool. The majority of GluR1 silver-gold particles were located in a pool more distal (>100 nm from the postsynaptic membrane) from RG synapses, forming a "residual" receptor pool that was insensitive to the expression of Ras mutants or CaMKII (Figure 4). Unexpectedly, active Ras or CaMKII drove GluR1 into PSD of CG

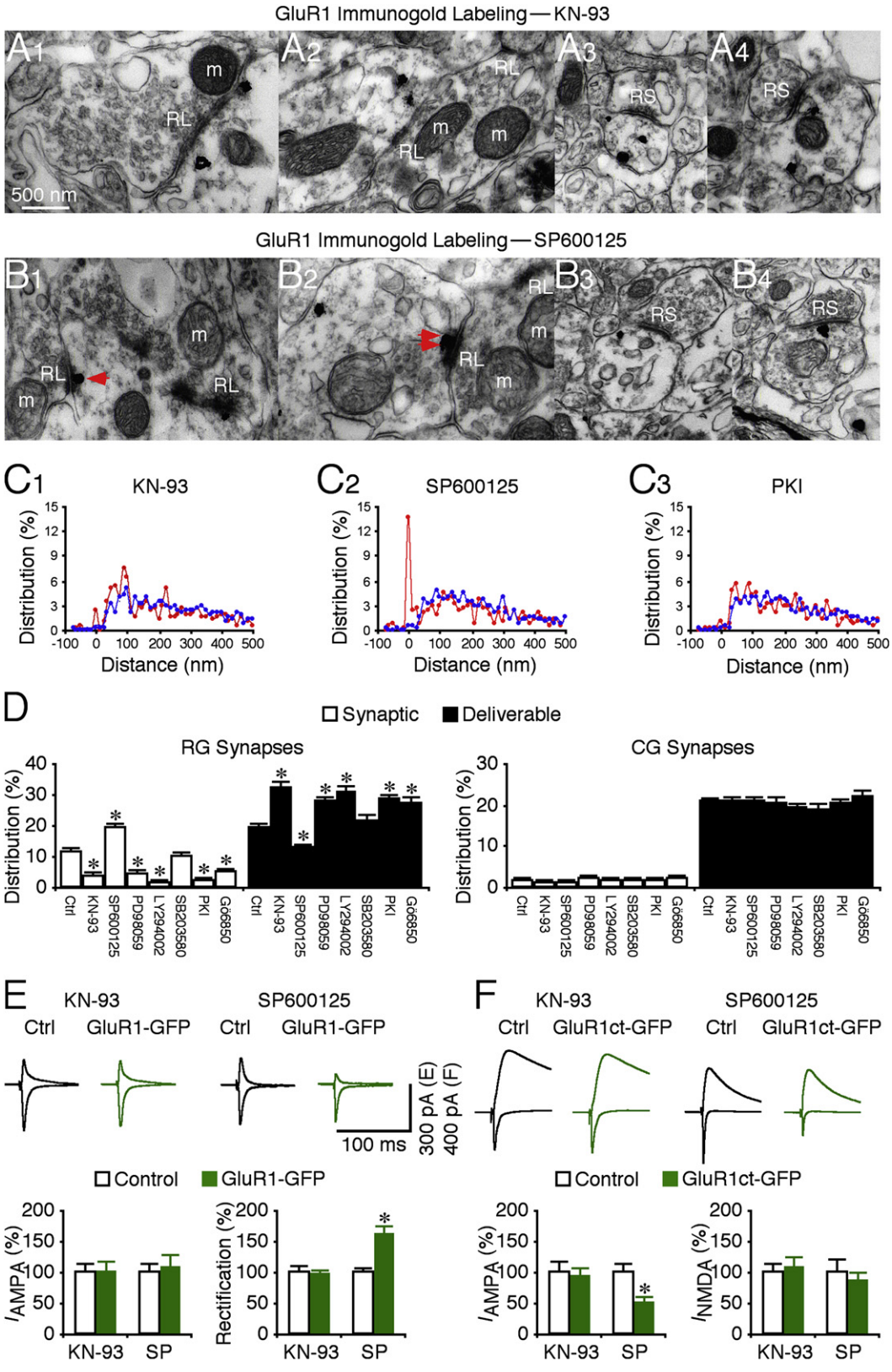
GluR1 Immunogold Labeling—KN-93
A1
A2
A3
A4
m
RL
RS
500 nm
GluR1 Immunogold Labeling—SP600125
B1
B2
B3
B4
C1
KN-93
C2
SP600125
C3
PKI
Distribution (%)
Distance (nm)
D
Synaptic
Deliverable
RG Synapses
CG Synapses
Ctrl
KN-93
SP600125
PD98059
LY294002
SB203580
PKI
G66850
E
F
KN-93
SP600125
Ctrl
GluR1-GFP
GluR1ct-GFP
100 ms
300 pA (E)
400 pA (F)
Control
GluR1-GFP
GluR1ct-GFP
I AMPA (%)
Rectification (%)
I NMDA (%)
SP

synapses and reduced GluR1 by an equal amount in the deliverable pool (Figures 4B, 4D, and 4E). These constructs had no effect on GluR1 in the residual pool at CG synapses (Figure 4E).

Rap2 Signals GluR1 Trafficking from Synaptic to Deliverable Pools

Rap2 signals synaptic removal of GluR1-containing AMPA-Rs (Zhu et al., 2005). In vivo viral expression of a constitutively active Rap2, Rap2(ca)-GFP, reduced the presence of GluR1 in PSD, whereas expression of a dominant-negative form of Rap2, Rap2(dn)-GFP, increased the presence of GluR1 in PSD at RG synapses (Figure 5). Correspondingly, Rap2(ca)-GFP and Rap2(dn)-GFP increased and decreased GluR1 by an equivalent amount in the deliverable pool of RG synapses, respectively (Figure 5). Expression of these constructs did not alter the relative amount of GluR1 in the residual pool at RG synapses (Figure 5). Rap2 mutants had no effect on GluR1 distribution at CG synapses (Figure 5), consistent with little GluR1 in PSD at these synapses. Rap1 signals synaptic removal of GluR2-containing AMPA-Rs (i.e., GluR2/3 AMPA-Rs) but has no effect on GluR1-containing AMPA-Rs (Zhu et al., 2002, 2005). As controls, expression of a constitutively active Rap1, Rap1(ca)-GFP, and a dominant-negative form of Rap1, Rap1(dn)-GFP, had no effects on the relative amount of GluR1 in the synaptic, deliverable, and residual pools at RG and CG synapses (Figures 5C and 5D). Together, these results suggest that Ras and Rap2 signal the opposite GluR1 interpool trafficking at RG synapses, whereas Rap1 has no role in the trafficking, congruent with the notion that Ras, Rap1, and Rap2 independently signal distinct AMPA-R trafficking events at synapses (Gu and Stornetta, 2007; Tada and Sheng, 2006; Zhu et al., 2002, 2005).

GluR1 Interpool Trafficking Requires Multiple Kinase Activity

To determine whether Ras, Rap1, and Rap2 signal GluR1 interpool trafficking via different kinase cascades, we examined the role of several kinases by in vivo injection of their specific inhibitors. CaMKII stimulates the Ras-MEK-MAPK and -PI3K-PKB signaling pathways, which together drive synaptic delivery of GluR1-containing AMPA-Rs (Hu et al., 2008; Qin et al., 2005; Zhu et al., 2002). Consistent with these findings, KN-93 (CaMKII inhibitor), PD98059 (MEK inhibitor), or LY294002 (PI3K inhibitor) reduced the number of GluR1 silver-gold particles in the synaptic pool and increased the same number of particles in the deliverable pool at RG synapses (Figures 6A, 6C, and 6D). The inhibitors had no effect on the number of GluR1 silver-gold particles in the residual pool at RG synapses or in the deliverable and residual pools at CG synapses (Figures 6A, 6C, and 6D). Rap2 removes synaptic GluR1-containing AMPA-Rs via JNK (Zhu et al., 2005). Consistent with this, SP600125 (JNK inhibitor) increased and reduced the number of GluR1 silver-gold particles in the synaptic pool and deliverable pools, respectively (Figures 6B and 6D). SP600125 had no effect on the particles in the other pools at geniculate synapses (Figures 6B and 6D). Rap1 stimulates p38 MAPK, which removes GluR2/3 AMPA-Rs (Hsieh et al., 2006; Zhu et al., 2002). As a control, in vivo application of SB203580 (p38 MAPK inhibitor) had no effect on the GluR1 distribution in the postsynaptic pools at geniculate synapses (Figures 6C and 6D). PKA and PKC are required for synaptic potentiation and GluR1 delivery (Shepherd and Huganir, 2007).

Figure 6. Multiple Kinases Regulate GluR1 Interpool Trafficking

(A and B) GluR1 immunogold labeling at synapses contacted by RL terminals in rats with LGN infusion of KN-93 (A1-3) and SP600125 (B1-3). Scale bar applies to (A) and (B).

(C) Relative distributions of GluR1 silver-gold particles at synapses contacted by RL (red) and RS (blue) terminals in rats with LGN infusion of KN-93 (C1: n = 464 for RL; n = 1,024 for RS), SP600125 (C2: n = 469 for RL; n = 1,156 for RS), and PKI (n = 551 for RL; n = 1,335 for RS). Relative distributions of GluR1 silver-gold particles at synapses contacted by RL and RS terminals in rats with LGN infusion of PD98059 (n = 479 for RL; n = 1068 for RS), LY294002 (n = 528 for RL; n = 1074 for RS), SB203580 (n = 556 for RL; n = 1196 for RS), and Gö6850 (n = 475 for RL; n = 976 for RS) were not shown.

(D) (Left) Average percentages of GluR1 silver-gold particles in synaptic and deliverable pools at synapses contacted by RL terminals in rats with LGN infusion of 50 μM KN-93 ($n = 10$, $p < 0.001$), 50 μM SP600125 ($n = 9$, $p < 0.001$), 200 μM PD98059 ($n = 10$, $p < 0.001$), 100 μM LY294002 ($n = 10$, $p < 0.001$), 20 μM SB203580 ($n = 10$, $p > 0.05$), 200 μM PKI 14-22 amide ($n = 10$, $p < 0.005$), or 100 nM biosindolylmaleimide (Gö6850, $n = 10$, $p < 0.05$), relative to normal control LGNs presented in Figure 2E. (Right) Average percentages of GluR1 silver-gold particles in synaptic and deliverable pools at synapses contacted by RS terminals in rats with LGN infusion of KN-93 ($n = 10$, $p > 0.05$), SP600125 ($n = 10$, $p > 0.05$), 200 μM PD98059 ($n = 10$, $p > 0.05$), LY294002 ($n = 10$, $p > 0.05$), SB203580 ($n = 10$, $p > 0.05$), PKI ($n = 10$, $p > 0.05$), or Gö6850 ($n = 10$, $p > 0.05$) were unchanged compared to normal control LGN. Note (not shown) that average percentages of GluR1 silver-gold particles in the residual pool at synapses contacted by RL ($n = 9$–12; $p > 0.05$) and RS ($n = 9$–12; $p > 0.05$) terminals were the same as that in normal LGN.

(E) (Upper) Evoked AMPA-R-mediated responses at retinogeniculate (RG) synapses from nonexpressing (Ctrl) and GluR1-GFP-expressing neurons in rats with LGN infusion of 50 μM KN-93 and 50 μM SP600125 recorded at −60 mV and +40 mV. (Lower left) RG AMPA responses in neurons expressing GluR1-GFP in rats with LGN infusion of KN-93 ($n = 12$; $p = 0.58$) or SP600125 ($n = 14$; $p = 0.64$) relative to neighboring control neurons. (Lower right) Rectification of RG AMPA responses in GluR1-GFP-expressing neurons in rats with LGN infusion of KN-93 ($n = 12$; $p = 0.39$) or SP600125 ($n = 14$; $p < 0.005$) relative to neighboring control cells. Note that GluR1ct-GFP-expressing neurons in rats with LGN infusion of SP600125 had more enhanced rectification compared to GluR1ct-GFP-expressing neurons in control rats (Ctrl: $n = 16$; SP: $n = 16$; $p < 0.005$; Mann-Whitney Rank Sum test; cf. Figure 2C).

(F) (Upper) Evoked AMPA-R- and NMDA-R-mediated responses at RG synapses from nonexpressing (Ctrl) and GluR1ct-GFP-expressing neurons in rats with LGN infusion of 50 μM KN-93 and 50 μM SP600125 recorded at −60 mV and +40 mV. (Lower left) RG AMPA responses in neurons expressing GluR1ct-GFP in rats with LGN infusion of KN-93 ($n = 17$; $p = 0.69$) or SP600125 ($n = 14$; $p < 0.005$) relative to neighboring control neurons. Note that GluR1ct-GFP-expressing neurons in rats with LGN infusion of SP600125 had more significantly reduced AMPA responses compared to GluR1ct-GFP-expressing neurons in control rats (Ctrl: $n = 16$; SP: $n = 14$; $p < 0.05$; Mann-Whitney Rank Sum test; cf. Figure 2D). (Lower right) RG NMDA responses in neurons expressing GluR1ct-GFP in rats with LGN infusion of KN-93 ($n = 17$; $p = 0.38$) or SP600125 ($n = 14$; $p = 0.64$) relative to neighboring control cells. AMPA-R and NMDA-R mediated current amplitude and standard errors were normalized to average values from control cells. Asterisks indicate statistical significance (Mann-Whitney Rank Sum or Wilcoxon test). See Supplemental Data for the values.

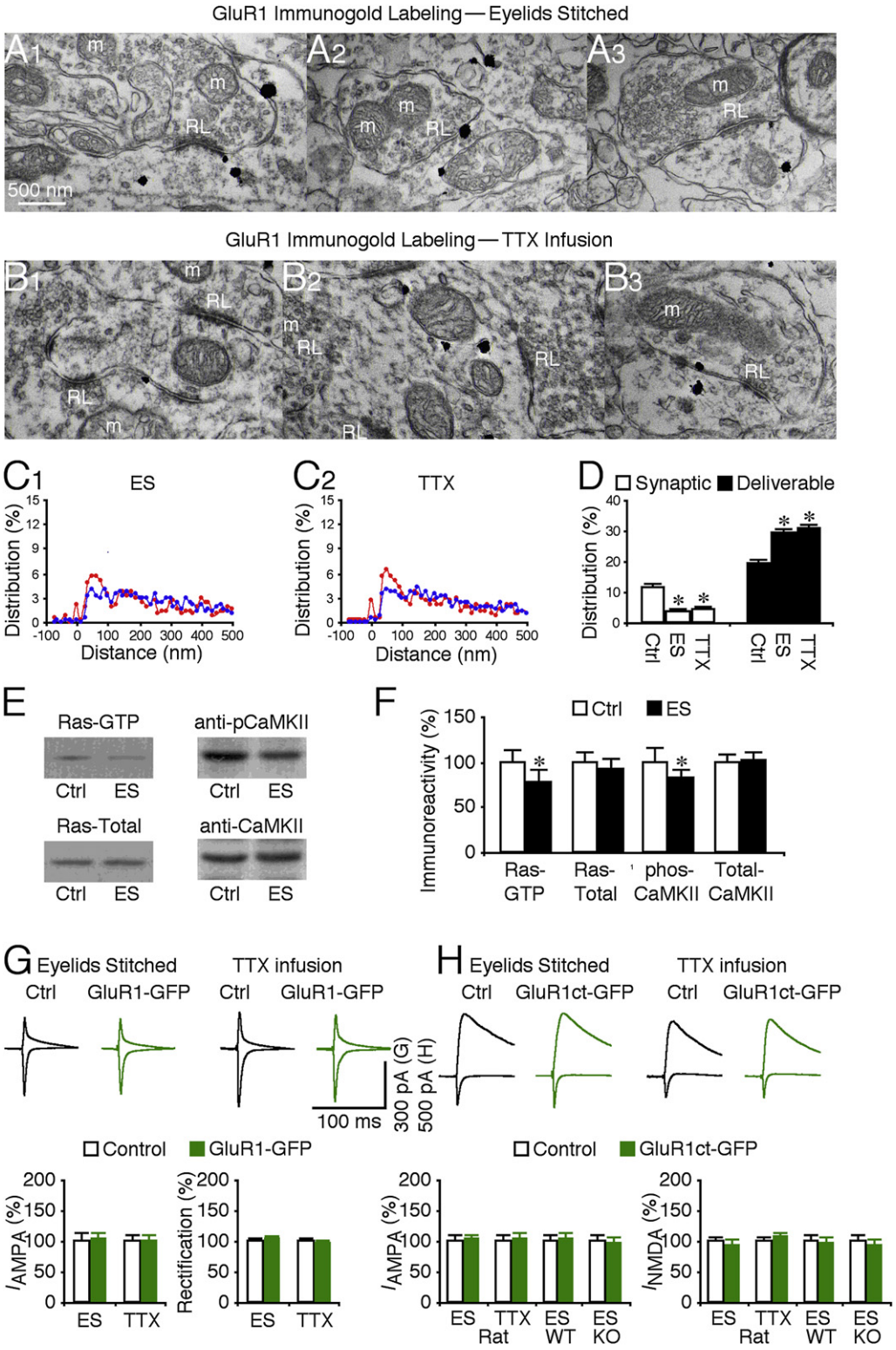

Figure 7. Vision-Dependent Activity Drives GluR1 Insertion at Retinogeniculate Synapses

(A and B) GluR1 immunogold labeling at synapses contacted by RL terminals in rats with eyelids stitched (ES, A1-3), and rats with LGN infusion of TTX (B1-3). Scale bar applies to (A) and (B).

(C) Relative distributions of GluR1 silver-gold particles at synapses contacted by RL (red) and RS (blue) terminals in rats with eyelids stitched (C1: n = 524 for RL; n = 1,334 for RS) and with LGN infusion of TTX (C2: n = 620 for RL; n = 1594 for RS).

PKI (PKA inhibitor) and Gö6850 (PKC inhibitor) reduced the number of GluR1 silver-gold particles in the synaptic pool and increased an equivalent number of particles in the deliverable pool at RG synapses (Figures 6C and 6D). PKI and Gö6850 had no effect on the GluR1 distribution in the other postsynaptic pools at geniculate synapses (Figures 6C and 6D). These results suggest that GluR1 interpool trafficking requires CaMKII, MEK, PI3K, PKA, and PKC, but not p38 MAPK.

To determine whether the CaMKII-delivered or JNK-removed GluR1 mediates transmission, we simultaneously injected KN-93 or SP600125 with the viral GluR1-GFP construct in LGN in vivo and subsequently examined synaptic transmission in vitro. KN-93 blocked and SP600125 potentiated the enhanced rectification of RG AMPA responses in GluR1-GFP-expressing neurons (Figure 6E; cf. Figure 2C), indicating that the CaMKII-delivered or JNK-removed GluR1-GFP mediates RG transmission. Next, we simultaneously injected KN-93 or SP600125 with the viral GluR1ct-GFP construct, which functioned as a dominant-negative construct to block synaptic trafficking of endogenous GluR1-containing AMPA-Rs and which reduced RG transmission (Figure 2D). KN-93 blocked and SP600125 potentiated the difference in RG AMPA responses between GluR1ct-GFP-expressing and nearby nonexpressing neurons (Figure 6F). These results suggest that KN-93 and SP600125 block synaptic trafficking of endogenous GluR1-containing AMPA-Rs that mediate RG transmission.

Experience-Dependent Activity Drives GluR1 Trafficking from Deliverable to Synaptic Pools

The above data indicate that GluR1 is transported to the deliverable pools of RG and CG synapses and that activation of Ras signaling can further drive GluR1-containing AMPA-Rs into PSD at both populations of geniculate synapses. Why then does GluR1 normally mediate RG but not CG transmission? To address this question, we investigated the regulation of forward trafficking of GluR1 from the deliverable pool into the synaptic pool at RG synapses. Previous studies have demonstrated that whisker-experience-dependent activity is essential for synaptic insertion of GluR1-containing AMPA-Rs in neurons of the barrel cortex (McCormack et al., 2006; Takahashi et al., 2003). In LGN, spontaneous or vision-dependent activity induces RG plasticity (Guido, 2008; Hooks and Chen, 2006). Thus, we manipulated the spontaneous and vision-experience-dependent activity in LGN. Blocking all synaptic activity by local infusion of TTX into LGN or selectively blocking vision-dependent activity by eye closure through eyelid suturing reduced the number of GluR1 silver-gold particles in PSD of RG synapses and increased the number of GluR1 silver-gold particles by the same proportion in the deliverable pool at these synapses (Figures 7A–7D). TTX and eyelid suturing did not alter the relative amount of GluR1 in the residual pool at RG synapses (Figure 7D). These results indicate that synaptic activity, particularly vision-dependent activity, is required for forward trafficking of GluR1 from the deliverable pool into PSD at RG synapses. Western blot analysis showed that eyelid suturing reduced the levels of GTP-bound (or active) Ras and phosphorylated (or active) CaMKII (Figures 7E and 7F), confirming the critical role of these signaling molecules in the forward GluR1 interpool trafficking from the deliverable to synaptic pools (Figure 4).

To determine whether the activity-dependent synaptic delivery of GluR1 mediates transmission, we virally expressed the GluR1-GFP construct in LGN in vivo, manipulated synaptic activity during the expression by TTX infusion and eye closure, and subsequently recorded RG transmission in vitro. TTX infusion and eye closure blocked the enhanced rectification of AMPA responses in GluR1-GFP-expressing neurons (Figure 7G; cf. Figure 2C), indicating blockade of recombinant GluR1-GFP trafficking into PSD to mediate RG transmission. Next, we in vivo microinjected the viral GluR1ct-GFP construct, which functioned as a dominant-negative construct to block synaptic trafficking of endogenous

(D) (Left) Average percentages of GluR1 silver-gold particles in synaptic and deliverable pools at synapses contacted by RL terminals in rats with eyelids stitched ($n = 10$, $p < 0.05$) or with LGN infusion of TTX ($n = 10$, $p < 0.001$) relative to normal control LGNs presented in Figure 2E. (Right) Average percentages of GluR1 silver-gold particles in synaptic and deliverable pools at synapses contacted by RS terminals in rats with eyelids stitched ($n = 10$, $p > 0.05$) or with LGN infusion of TTX ($n = 10$, $p > 0.05$) were unchanged compared to normal control LGN. Note (not shown) that average percentages of GluR1 silver-gold particles in the residual pool at synapses contacted by RL ($n = 10$–12; $p > 0.05$) and RS ($n = 10$–12; $p > 0.05$) terminals were the same as that in normal LGN.

(E) Western blots of GTP-bound active Ras, total Ras, phosphorylated CaMKII, and total CaMKII in LGN from normal control rats and rats with eyelids stitched. For each set of cell lysates, 35 μg protein was used to purify and blot GTP-bound Ras, 7.5 μg protein was used to directly blot total Ras, and 45 μg protein was used to blot phos-CaMKII and total CaMKII.

(F) Relative amounts of Ras-GTP ($n = 12$; $p < 0.05$), total Ras ($n = 12$; $p = 0.40$), phos-CaMKII ($n = 16$; $p < 0.01$), and total CaMKII ($n = 16$; $p = 0.47$) in LGN from normal control rats and rats with eyelids stitched. The relative values and standard errors were normalized to average amounts of Ras-GTP, total Ras, phos-CaMKII, or total CaMKII in LGN from normal control rats.

(G) (Upper) Evoked AMPA-R-mediated responses at retinogeniculate (RG) synapses from nonexpressing (Ctrl) and GluR1-GFP-expressing neurons in rats with eyelids stitched and rats with LGN infusion of TTX recorded at −60 mV and +40 mV. (Lower left) RG AMPA responses in neurons expressing GluR1-GFP in rats with eyelids stitched ($n = 22$; $p = 0.88$) or with LGN infusion of TTX ($n = 15$; $p = 0.91$) relative to neighboring control neurons. (Lower right) Rectification of RG AMPA responses in GluR1-GFP-expressing neurons in rats with eyelids stitched ($n = 22$; $p = 0.57$) or with LGN infusion of TTX ($n = 15$; $p = 0.14$) relative to neighboring control cells.

(H) (Upper) Evoked AMPA-R- and NMDA-R-mediated responses at RG synapses from nonexpressing (Ctrl) and GluR1ct-GFP-expressing neurons in rats with eyelids stitched and with LGN infusion of TTX recorded at −60 mV and +40 mV. (Lower left) RG AMPA responses in neurons expressing GluR1ct-GFP in rats with eyelids stitched ($n = 13$; $p = 0.65$), in rats with LGN infusion of TTX ($n = 14$; $p = 0.64$), in wild-type (WT) mice with eyelids stitched ($n = 17$; $p = 0.80$), or in *GluR1* knockout (KO) mice with eyelids stitched ($n = 17$; $p = 0.72$) relative to neighboring control neurons. (Lower right) RG NMDA responses in neurons expressing GluR1ct-GFP in rats with eyelids stitched ($n = 13$; $p = 0.38$), in rats with LGN infusion of TTX ($n = 14$; $p = 0.25$), in wild-type (WT) mice with eyelids stitched ($n = 17$; $p = 0.69$), or in *GluR1* knockout (KO) mice with eyelids stitched ($n = 17$; $p = 0.44$) relative to neighboring control cells. AMPA-R- and NMDA-R-mediated current amplitude and standard errors were normalized to average values from control cells. Asterisks indicate statistical significance (Mann-Whitney Rank Sum or Wilcoxon test). See Supplemental Data for the values.

GluR1-containing AMPA-Rs and which reduced RG transmission (Figure 2D). With TTX infusion and eye closure applied during the GluR1ct-GFP expression, the difference in RG AMPA responses between GluR1ct-GFP-expressing and nearby nonexpressing neurons was eliminated (Figure 7H). The difference in RG AMPA responses between GluR1ct-GFP-expressing and nearby nonexpressing neurons was also eliminated in wild-type and *GluR1* knockout mice (Figure 7H), suggesting that eye closure, expression of GluR1ct-GFP, and *GluR1* knockout all block GluR1-dependent synaptic plasticity. Together, these results suggest that TTX infusion and eye closure block synaptic trafficking of endogenous GluR1-containing AMPA-Rs that mediate RG transmission in control nonexpressing neurons.

Electrophysiological studies have shown that expression of GluR1ct-GFP selectively blocks synaptic delivery of endogenous GluR1 (Kessels and Malinow, 2009). We wished to confirm the finding anatomically. Expression of GluR1ct-GFP reduced the presence of GluR1 in PSD and increased GluR1 by an equivalent amount in the deliverable pool of RG synapses (Figures 8A, 8C, and 8D). The same results were obtained in animals with eyelids stitched (Figures 8A, 8C, and 8D), confirming the occlusion of GluR1-dependent plasticity between the GluR1ct-GFP expression and eye closure (cf. Figures 2D and 7H). Electrophysiology studies have demonstrated that the rectified recombinant GluR1-GFP behaves in the same manner as endogenous heteromeric GluR1-containing AMPA-Rs during synaptic delivery (Kessels and Malinow, 2009). Consistent with this idea, immunogold labeling showed that GluR1-GFP silver-gold particles were distributed in PSD or synaptic pool (~12%), deliverable pool (~18%), and residual pool (~70%), and eye closure resulted in the majority of synaptic GluR1-GFP silver-gold particles appearing in the deliverable pool (Figures 8B–8D). Together, these results provide an independent anatomical confirmation of the notion that GluR1ct-GFP and GluR1-GFP blocks and mimics synaptic trafficking of endogenous GluR1-containing AMPA-Rs, respectively. Collectively, these results indicate that vision-dependent activity drives forward trafficking of GluR1-containing AMPA-Rs from the deliverable pool into the synaptic pool to mediate functional RG transmission.

CG inputs onto LGN seem more effective in slowly shifting membrane potential than in initiating action potentials, whereas vision-dependent retinal inputs onto LGN are efficient in triggering time-locked spikes in geniculate cells (Augustinaite and Heggelund, 2007; Steriade et al., 1997; Usrey et al., 1998; Wang et al., 2006). Because active Ras and CaMKII can drive GluR1 into PSD of CG synapses, we speculated that the signaling machinery (at least downstream of CaMKII) required for forward trafficking of GluR1 is present at CG synapses. However, the signaling machinery is normally dormant at these synapses since vision-dependent suprathreshold synaptic activity, which may be required to activate CaMKII/Ras signaling, is missing. To test this idea, we selectively stimulated the CG pathway in the in vitro LGN preparation using 200 paired pulses (with a 20 ms interpulse interval) delivered at 2 Hz. This stimulation paradigm, which is highly efficient in driving geniculate neurons to generate spikes in the RG pathway (Usrey et al., 1998), was effective in eliciting action potentials in geniculate neurons when applied in the CG pathway (Figure S2). Subsequent immunolabeling showed that CG stimuli increased the number of GluR1 silver-gold particles in PSD of CG synapses and reduced the number of GluR1 silver-gold particles by an equal amount in the deliverable pool of these synapses (Figures 9A–9D). Including an NMDA-R blocker, APV, in the bath solution during the stimulation blocked the effect, indicating the requirement of NMDA-R activation. These manipulations did not alter the relative amount of GluR1 in the residual pool at CG synapses (Figure 9D).

To test whether the newly delivered GluR1 in PSD mediates CG transmission, we virally expressed GluR1-GFP and GluR1ct-GFP in LGN in vivo and subsequently recorded CG responses in vitro. The CG stimulation resulted in enhanced rectification of CG AMPA responses in GluR1-GFP-expressing neurons and reduced CG AMPA responses in GluR1ct-GFP-expressing neurons (Figures 9E and 9F). Bath application of APV blocked the effects (Figures 9E and 9F). The results indicate that, as with AMPA-Rs in the deliverable pool at RG synapses, those at CG synapses can be delivered into synapses to mediate transmission. Collectively, these results suggest that vision-dependent activity is responsible for the selective delivery of GluR1-containing AMPA-Rs into RG synapses but not into CG synapses.

DISCUSSION

In this study, we have demonstrated that GluR1-containing AMPA-Rs, which have slow gating kinetics, selectively mediate transmission at RG but not CG synapses in single geniculate neurons. In addition, only ~12% of GluR1 receptors are located within PSD at RG synapses, forming a synaptic pool of AMPA-Rs. The majority of GluR1 receptors are located in the nearby deliverable (~18%) and residual (~70%) pools. Moreover, Ras and Rap2 signal bidirectional GluR1 trafficking between the deliverable and synaptic pools; the processes effectively enhance and reduce synaptic strength, respectively. Finally, we show that nonselective transportation of GluR1 to both RG and CG synapses followed by preferential incorporation of GluR1 into RG synapses mediates synapse-specific delivery of GluR1.

Synapse-Specific AMPA-R Trafficking

Synapse-specific incorporation of different AMPA-R subunits, which exhibit distinct gating properties, can have profound impacts on synaptic integration and information processing (Gardner et al., 2001; Geiger et al., 1997; Jonas, 2000; Toth and McBain, 1998). The slow, more GluR1-mediated RG EPSCs, combined with their large amplitude (Chen and Regehr, 2000; Turner and Salt, 1998), are crucial for generating sufficient charge to initiate action potentials with precise timing to faithfully relay ascending sensory information (Augustinaite and Heggelund, 2007; Liu and Chen, 2008). On the other hand, the fast, mainly GluR4-mediated CG EPSCs, which are small in amplitude (Turner and Salt, 1998), provide limited current charge. These small inputs, which become even smaller and more prolonged somatic depolarizations due to the severe dendritic filtering, are well suited for slow adjustment of the membrane potential in geniculate neurons (Steriade et al., 1997; Wang et al., 2006). Thus, differential incorporation of GluR1 and GluR4 allows RG and CG synapses to function as efficient drivers and modulators to relay

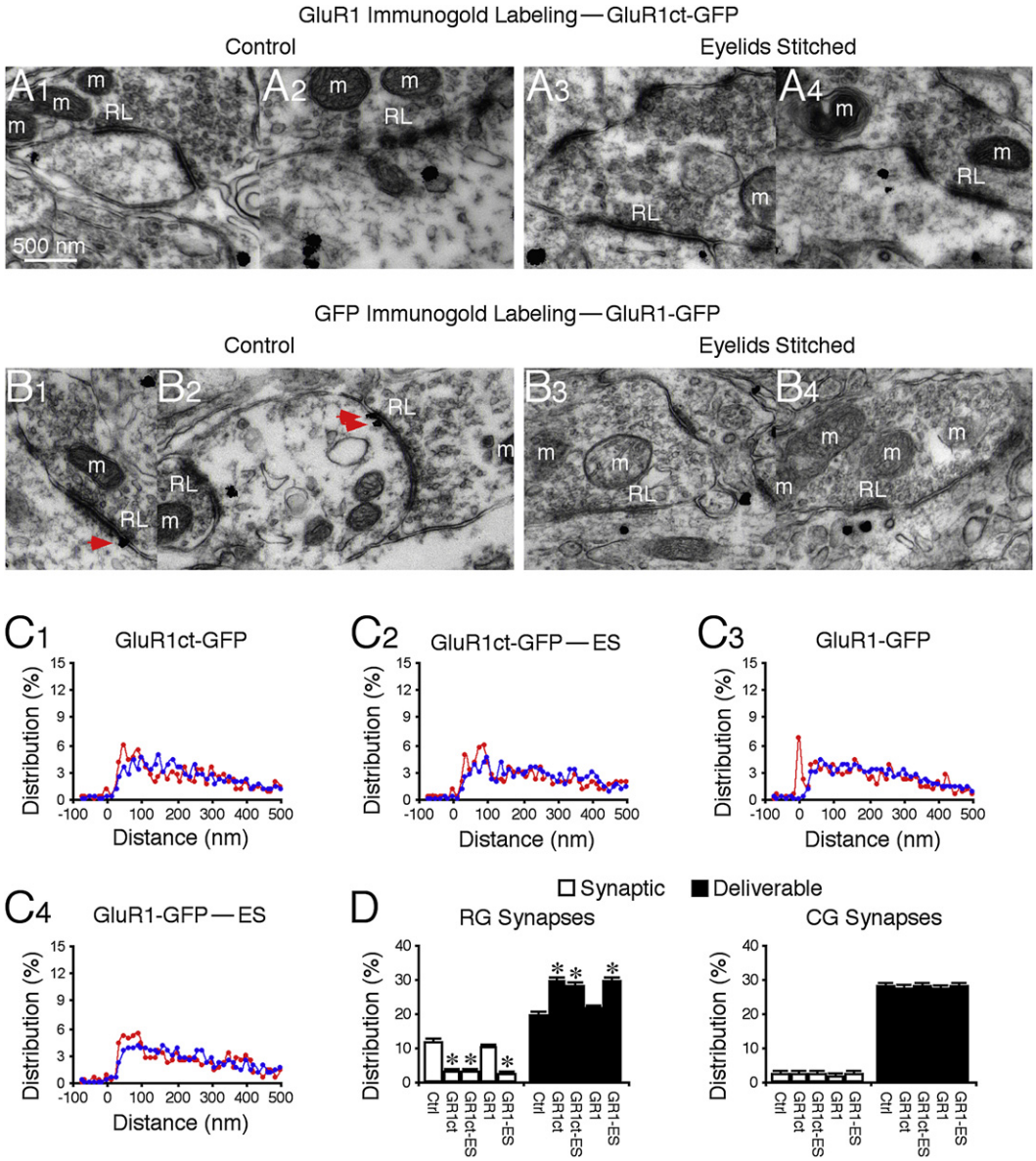

Figure 8. Vision-Dependent Activity Drives Synaptic Insertion of Endogenous and Recombinant GluR1

(A and B) GluR1 immunogold labeling at synapses contacted by RL terminals in GluR1ct-GFP-expressing neurons from control rats (Ctrl, A1-2) and rats with eyelids stitched (ES, A3-4), and GFP immunogold labeling at synapses contacted by RL terminals in GluR1-GFP-expressing neurons from control rats (Ctrl, B1-2) and rats with eyelids stitched (ES, B3-4). Red arrows point to silver-enhanced gold particles associated with PSDs postsynaptic to RL terminals. Scale bar applies to (A) and (B).

(C) Relative distributions of GluR1 silver-gold particles at synapses contacted by RL (red) and RS (blue) terminals in GluR1ct-GFP-expressing neurons from control rats (C1: n = 499 for RL; n = 1154 for RS) and rats with eyelids stitched (C2: n = 508 for RL; n = 1196 for RS), and GFP silver-gold particles at synapses contacted by RL (red) and RS (blue) terminals in GluR1-GFP-expressing neurons from control rats (C3: n = 487 for RL; n = 1161 for RS) and rats with eyelids stitched (C4: n = 524 for RL; n = 1168 for RS).

(D) (Left) Average percentages of GluR1 or GFP silver-gold particles in synaptic and deliverable pools at synapses contacted by RL terminals in GluR1ct-GFP neurons from control rats ($n = 10$, $p < 0.001$) and rats with eyelids stitched ($n = 10$, $p < 0.005$) and in GluR1-GFP neurons from control rats ($n = 10$, $p > 0.05$) and rats with eyelids stitched ($n = 10$, $p > 0.05$) relative to normal control LGNs presented in Figure 2E. Note no significant differences for average percentages of GluR1 silver-gold particles in synaptic and deliverable pools at synapses contacted by RL terminals in GluR1ct-GFP neurons from control rats and those from rats with eyelids stitched ($p > 0.05$), but significant differences for average percentages of GFP silver-gold particles in synaptic and deliverable pools at synapses contacted by RL terminals in GluR1-GFP neurons from control rats and those from rats with eyelids stitched ($p < 0.005$). (Right) Average percentages of GluR1 or GFP silver-gold particles in synaptic and deliverable pools at synapses contacted by RS terminals in GluR1ct-GFP neurons from control rats ($n = 10$, $p > 0.05$) and rats with eyelids stitched ($n = 10$, $p > 0.05$) and in GluR1-GFP neurons from control rats ($n = 10$, $p > 0.05$) and rats with eyelids stitched ($n = 10$, $p > 0.05$) were unchanged compared to normal control LGN. Note (not shown) that average percentages of GluR1 or GFP silver-gold particles in the residual pool at synapses contacted by RL ($n = 9–12$; $p > 0.05$) and RS ($n = 9–12$; $p > 0.05$) terminals were the same as that in normal LGN. Asterisks indicate statistical significance (Mann-Whitney Rank Sum test). See Supplemental Data for the values.

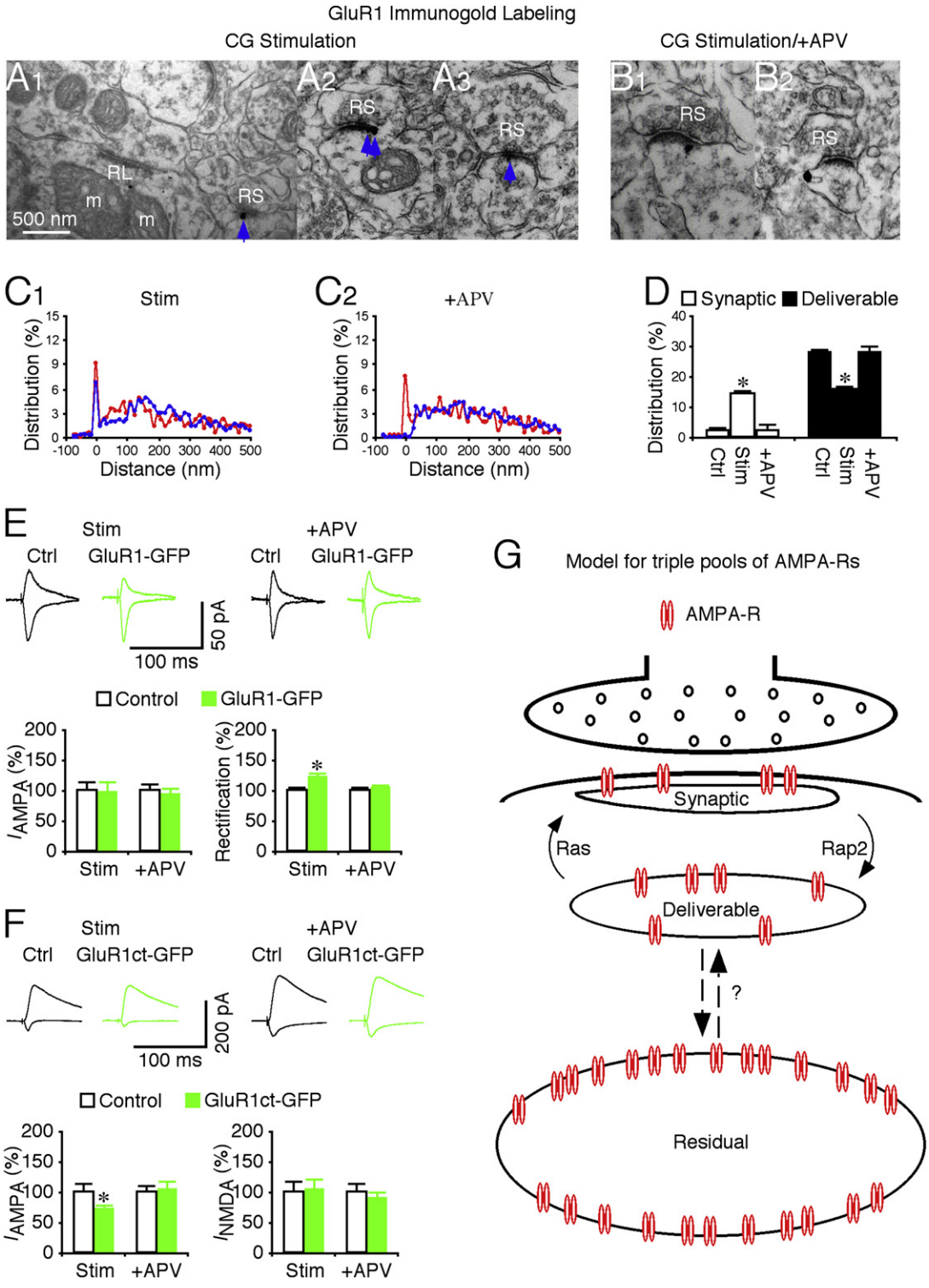

Figure 9. Synaptic Stimulation Drives GluR1 Insertion at Corticogeniculate Synapses

(A and B) GluR1 immunogold labeling at synapses contacted by RS terminals in LGN after synaptic stimulation of CG pathway in normal bath solution (A1-3), and bath solution with additional 100 μM DL-APV (B1-2). Scale bar applies to (A) and (B).

(C) Relative distributions of GluR1 silver-gold particles at synapses contacted by RL (red) and RS (blue) terminals in LGN after synaptic stimulation of CG pathway in normal bath solution (C1: n = 575 for RL; n = 1381 for RS), and bath solution with 100 μM DL-APV (C2: n = 506 for RL; n = 1236 for RS).

visual information and modulate RG transmission in LGN, respectively (Sherman and Guillery, 2002; Steriade et al., 1997).

Multiple Postsynaptic AMPA-R Pools

We report here an intricate AMPA-R pooling system at postsynaptic sites of geniculate neurons, consisting of three anatomically and physiologically distinguished AMPA-R groups (Figure 9G), which resembles the triple vesicle pool system at presynaptic sites (Rizzoli and Betz, 2005; Zucker and Regehr, 2002). About 12% of AMPA-Rs collect within PSD to form synaptic AMPA-Rs, which mediate functional transmission. Another ~18% of AMPA-Rs cluster close to PSD (within ~30–100 nm from the postsynaptic membrane) in the deliverable pool that supplies and recycles receptors for the synaptic pool, functionally matching the pool residing in recycling endosomes at hippocampal synapses (Park et al., 2004, 2006). However, the majority of AMPA-Rs are located more distally from the postsynaptic membrane (>100 nm), forming a pool of receptors that seems insensitive to synaptic activity, CaMKII, Ras, and Rap2 signaling. The exact functional role of the residual pool in synaptic transmission and plasticity remains unknown, but it is likely that the pool may supply and exchange the deliverable and synaptic pools with newly synthesized AMPA-Rs to maintain normal protein turnover and/or dispatch additional AMPA-Rs into deliverable and synaptic pools to increase the capacity of synaptic plasticity when needed (see below).

GluR1 Trafficking between Synaptic and Deliverable Pools

We report here that Ras activity stimulates the forward GluR1 trafficking, Rap2 activity stimulates the reverse GluR1 trafficking, and Rap1 activity has no effect on the GluR1 trafficking between the deliverable and synaptic pools. Moreover, the forward trafficking of GluR1 requires MEK and PI3K activity, whereas the reverse transport requires JNK activity. These results confirm the notion that Ras, Rap1, and Rap2 signal independently (Fu et al., 2007; Nonaka et al., 2008; Zhu et al., 2002, 2005). The findings also suggest a model in which Ras and Rap2 control synaptic efficacy in parallel by regulating the relative distribution of GluR1 in the synaptic and deliverable pools (Figure 9G), and together the sizes of these pools set the capacity of synaptic plasticity (cf. McCormack et al., 2006).

Pharmacology experiments, although never conclusive, support the notion that CaMKII, PKA, and PKC are crucial for synaptic potentiation (Boehm et al., 2006; Ehlers, 2000; Esteban et al., 2003; Gao et al., 2006; Malenka et al., 1989; Malinow et al., 1989; Oh et al., 2006; Silva et al., 1992). Because CaMKII, PKA, and PKC can phosphorylate S831, S845, and S818 of GluR1, respectively (hence called the "CaMKII site," "PKA site," and "PKC site") (Shepherd and Huganir, 2007), one simple, generally assumed model is that CaMKII, PKA, and PKC control GluR1 trafficking by directly phosphorylating these sites. Alternatively, CaMKII may relay synaptic NMDA-R activity via Ras to control synaptic delivery of AMPA-Rs during synaptic potentiation (Hu et al., 2008; Zhu et al., 2002). Consistent with this idea that CaMKII signals upstream of Ras, imaging studies have shown that LTP-inducing stimuli and NMDA-R activation briefly stimulate CaMKII activity, prior to Ras activation (Yasuda et al., 2006; S.-J. Lee et al., 2008, Society for Neuroscience, abstract). The relative upstream location of CaMKII in the NMDA-R-stimulated kinase cascades suggests that CaMKII may function as a signaling divergence molecule that, in addition to signals through the Ras pathways to control AMPA-R trafficking, may also signal via other pathways to control the other plasticity-related events, such as spine growth (Okamoto et al., 2007; Steiner et al., 2008).

As an alternative to the direct phosphorylation model, PKA and PKC may modulate MAPK and other signaling pathways by forming multiple protein complexes with signaling molecules via scaffold proteins (i.e., A-kinase anchoring proteins) (Luttrell, 2003; Smith et al., 2006), and may thus modulate a very large number of cellular processes (Steinberg, 2008; Tasken and Aandahl, 2004). Indeed, PKA and PKC may play two essential roles in the regulation of MAPK signaling (Impey et al., 1998; Liebmann, 2001; Roberson et al., 1999). First, basal PKA and PKC activities are required for normal MAPK signaling (or basal MAPK activity), due presumably to abundant PKA and PKC sites in molecules in the signaling pathways. The finding explains why PKA and PKC are required for synaptic potentiation given that MAPK signaling is crucial for GluR1 phosphorylation and synaptic delivery during

(D) (Left) Average percentages of GluR1 silver-gold particles in synaptic and deliverable pools at synapses contacted by RS terminals in LGN after synaptic stimulation of CG pathway in normal bath solution ($n = 10$, $p < 0.001$) or bath solution with 100 μM DL-APV ($n = 10$, $p > 0.05$) relative to normal control LGNs presented in Figure 2E. (Right) Average percentages of GluR1 silver-gold particles in synaptic and deliverable pools at synapses contacted by RL terminals in LGN after synaptic stimulation of CG pathway in normal bath solution ($n = 10$, $p > 0.05$) or bath solution with 100 μM DL-APV ($n = 10$, $p > 0.05$) were unchanged compared to normal control LGN. Note (not shown) that average percentages of GluR1 silver-gold particles in the residual pool at synapses contacted by RL ($n = 10–12$; $p > 0.05$) and RS ($n = 10–12$; $p > 0.05$) terminals were the same as that in normal LGN.

(E) (Upper) Evoked AMPA-R-mediated responses at corticogeniculate (CG) synapses from nonexpressing (Ctrl) and GluR1-GFP-expressing neurons in rats after synaptic stimulation of CG pathway in normal bath solution and bath solution with DL-APV recorded at −60 mV and +40 mV. (Lower left) CG AMPA responses in neurons expressing GluR1-GFP in rats after synaptic stimulation of CG pathway in normal bath solution ($n = 19$; $p = 0.72$) or bath solution with 100 μM DL-APV ($n = 22$; $p = 0.76$) relative to neighboring control neurons. (Lower right) Rectification of CG AMPA responses in GluR1-GFP-expressing neurons in rats after synaptic stimulation of CG pathway in normal bath solution ($n = 19$; $p < 0.05$) or bath solution with 100 μM DL-APV ($n = 22$; $p = 0.66$) relative to neighboring control cells.

(F) (Upper) Evoked AMPA-R- and NMDA-R-mediated responses at CG synapses from nonexpressing (Ctrl) and GluR1ct-GFP-expressing neurons in rats after synaptic stimulation of CG pathway in normal bath solution and bath solution with DL-APV recorded at −60 mV and +40 mV. (Lower left) CG AMPA responses in neurons expressing GluR1ct-GFP in rats after synaptic stimulation of CG pathway in normal bath solution ($n = 16$; $p < 0.05$) or bath solution with 100 μM DL-APV ($n = 16$; $p = 0.84$) relative to neighboring control neurons. (Lower right) CG NMDA responses in neurons expressing GluR1ct-GFP in rats after synaptic stimulation of CG pathway in normal bath solution ($n = 16$; $p = 0.96$) or bath solution with 100 μM DL-APV ($n = 16$; $p = 0.33$) relative to neighboring control cells. AMPA-R- and NMDA-R-mediated current amplitude and standard errors were normalized to average values from control cells. Asterisks indicate statistical significance (Mann-Whitney Rank Sum or Wilcoxon test). See Supplemental Data for the values.

(G) Model for triple AMPA-R pools at synapses.

LTP (English and Sweatt, 1997; Hu et al., 2008; Qin et al., 2005; Zhu et al., 2002). Moreover, PKA and PKC stimulate a much higher level of MAPK activation than NMDA-R activation, LTP-inducing stimuli in slices, or experience-dependent activity in vivo. Interestingly, the PKA- or PKC-stimulated synaptic enhancement is also much larger than those induced by LTP-inducing stimuli or experience-dependent synaptic activity in intact brains (Boehm et al., 2006; Esteban et al., 2003; Oh et al., 2006). Together, these findings suggest that PKA and PKC permissively (from upstream) regulate the gain of MAPK signaling to control the capacity of synaptic potentiation. One obvious puzzle is how PKA and PKC can induce the unusually large synaptic potentiation, given the limited size of the deliverable AMPA-R pool. One possibility is that PKA and PKC agonists stimulate synaptic delivery of large-conductance GluR2-lacking AMPA-Rs (Isaac et al., 2007) and/or recruit additional AMPA-Rs from the residual pool. It should be noted that currently available techniques are not ideal to precisely position a kinase in kinase cascades (i.e., sequential or parallel and downstream or upstream) and determine its function (i.e., permissive or imperative) in subcellular compartments at synapses in physiological conditions. Thus, fully addressing these issues has to wait for the development of high-resolution, simultaneous monitoring techniques.

Mechanism for Synapse-Specific AMPA-R Delivery

Proper functioning of a cell requires the precise placement of membrane proteins at strategic locations in subcellular domains (Lai and Jan, 2006; Mellman and Nelson, 2008; Vacher et al., 2008). Many membrane proteins employ the preferential transportation and incorporation mechanism to travel to the major cellular domains, e.g., the axon or dendrite in neurons (Matsuda et al., 2008; Sampo et al., 2003; Setou et al., 2000). However, typical membrane proteins are unevenly distributed, and they often present only in selective subcellular membrane compartment(s) of these domains (Hoffman et al., 1997; Pelkey et al., 2006; Schaefer et al., 2007; Zhu, 2000). It seems unlikely that the limited intracellular transportation systems can use this scheme to selectively sort and deliver all these proteins to their functional destinations. The scheme of nonselective incorporation and preferential retention mechanism may be competent for the task of subcellular domain targeting. For example, several synaptic membrane proteins are functionally incorporated into the membrane throughout the axon or dendrite, and they appear to be preferentially retained in synapses after synaptogenesis (Friedman et al., 2000; Washbourne et al., 2004). The functional significance of the initial incorporation of membrane proteins into "inappropriate" locations is still unclear, but the process could be important for presorting or receiving trophic signals for regulation of development and plasticity (Huang and Scheiffele, 2008; McAllister, 2007).

Here we report a nonselective transportation and preferential incorporation mechanism that allows GluR1 to travel to and be incorporated in the membrane of RG synapses but avoid incorporation into inappropriate locations, i.e., CG synapses. GluR1 is nonselectively transported to both proximally located RG synapses and distally located CG synapses and then preferentially incorporated into RG synapses. Interestingly, GluR1 silver-gold particles are occasionally present on the plasma membrane nearby PSD at RG synapses (but rarely at CG synapses; our unpublished data). It is tempting to speculate that in the intact brain GluR1 also travels in and out of synapses via perisynaptic plasma membrane as suggested by in vitro studies (Ehlers, 2000; Ehlers et al., 2007; Gao et al., 2006; Oh et al., 2006; Serulle et al., 2007; Yang et al., 2008). Because blocking Rap2 or JNK signaling, which blocks synaptic removal of GluR1 (Zhu et al., 2005), does not cause synaptic accumulation of GluR1 at CG synapses, preferential retention/endocytosis is unlikely to be the correct mechanism. Rather, the vision-dependent activity pattern, present in the RG pathway but absent in the CG pathway, preferentially drives forward trafficking of GluR1-containing AMPA-Rs from the deliverable pool into the synaptic pool to mediate RG transmission and thus governs synapse-specific targeting of GluR1 in geniculate neurons. Thus, the Hebbian positive feedback mechanism not only controls synaptic efficacy by scaling the amount of synaptic incorporation of GluR1 at RG synapses but also effectively prevents synaptic incorporation of GluR1 at CG synapses. The nonselective transportation and preferential incorporation scheme suggested by our data, perhaps in combination with the other schemes to enhance sorting accuracy (Matsuda et al., 2008; Schuck and Simons, 2004), may be generalized to other proteins and in other cell types to solve the problem of differential sorting and targeting.

EXPERIMENTAL PROCEDURES

Biochemical Analyses

Tissue extracts were prepared by slicing the brain blocks containing LGN and hippocampus from P15–P27 rats, followed by dissecting, freezing (with dry ice), and homogenizing the geniculate and hippocampal tissues (Zhu et al., 2000, 2002). Western blots were quantified by chemiluminescence and densitometric scanning of the films under linear exposure conditions.

Recombinant Protein Expression

Animal preparation and in vivo expression of recombinant proteins in LGN followed procedures of previous studies (Hu et al., 2008; McCormack et al., 2006; Qin et al., 2005). 15 ± 3 hr after expression, the infected brains were isolated, and in vitro LGN slices were prepared as previously described (Kielland et al., 2006; Turner and Salt, 1998). To preserve both sensory and cortical inputs, we first made sections forming an angle of ~10°–15° to the midsagittal plane and angled outward by ~15°–20° in the mediolateral plane. Then, the medial aspect of each brain half was glued onto the stage of a microslicer and cut into 400 μm thick slices.

Immunoelectron Microscopy

Immunolabeling was carried out following the procedures of previous studies (Erisir and Harris, 2003; Hettinger et al., 2001). RL and RS terminals were classified according to the criteria used in our previous studies (Erisir et al., 1997; Kielland et al., 2006). Using presynaptic vesicular glutamate transporter 1 as an immunomarker for glutamatergic terminals (Fremeau et al., 2001), we found that 64.17% ± 0.01% (n = 9) of RS terminals are from CG afferents in rats (Figure S3). Synapses contacted by RL and RS terminals typically had 1–20 silver-enhanced gold particles. Given that these synapses had PSDs with the same thickness (RL: 26.3 ± 0.3 nm, n = 283; RS: 28.5 ± 1.1 nm, n = 655; $p = 0.83$), we counted all particles within 500 nm from the postsynaptic membrane and classified those within the concentric rings of −6.25 to 31.25 nm from the postsynaptic membrane into the synaptic pool, and those of 31.25 to 106.25 nm into the deliverable pool.

Electrophysiology

Simultaneous whole-cell in vitro recordings were obtained from pairs of neighboring infected and noninfected thalamocortical neurons, under visual guidance using fluorescence and transmitted light illumination as described previously (Perreault et al., 2003; Zhu et al., 2000). Expressing and nonexpressing geniculate neurons had the same basic membrane properties (Figure S4). CG stimulation in vitro was delivered at 2 Hz to take advantage of a presynaptic NMDA-R-independent potentiation mechanism (Castro-Alamancos and Calcagnotto, 1999). Results are reported as mean ± SEM. Statistical significances of the means ($p < 0.05$) were determined using Wilcoxon and Mann-Whitney Rank Sum nonparametric tests for paired and unpaired samples, respectively.

See the Supplemental Data for the detailed experimental procedures.

SUPPLEMENTAL DATA

The Supplemental Data include Supplemental Experimental Procedures, four supplemental figures, data values for Figures 1–9, and a supplemental reference and can be found with this article online at http://www.neuron.org/supplemental/S0896-6273(09)00198-6.

ACKNOWLEDGMENTS

We thank Drs. Martha Bickford, Jim Casavona, Chris McBain, Sacha Nelson, Ruth Stornetta, Bettina Winckler, and Ling-gang Wu for helpful discussions; members of the Zhu laboratory for comments and helping with several experiments; Dr. Pavel Osten for anti-GluR2L; Drs. Alev Erisir, Patrice Guyenet, and Arild Nja for use of lab resources and consultation. A.K. was a visiting graduate student supported in part by a University of Virginia Research and Development Award, and this paper is the part of a dissertation in partial fulfillment of the requirements of his Ph.D. degree at the University of Oslo, Oslo, Norway. The additional support of this project is from the DOD, NIH, and Norwegian Research Council.

Accepted: March 3, 2009
Published: April 15, 2009

REFERENCES

Augustinaite, S., and Heggelund, P. (2007). Changes in firing pattern of lateral geniculate neurons caused by membrane potential dependent modulation of retinal input through NMDA receptors. J. Physiol. *582*, 297–315.

Boehm, J., Kang, M.G., Johnson, R.C., Esteban, J., Huganir, R.L., and Malinow, R. (2006). Synaptic incorporation of AMPA receptors during LTP is controlled by a PKC phosphorylation site on GluR1. Neuron *51*, 213–225.

Burack, M.A., Silverman, M.A., and Banker, G. (2000). The role of selective transport in neuronal protein sorting. Neuron *26*, 465–472.

Casanova, J.E., Breitfeld, P.P., Ross, S.A., and Mostov, K.E. (1990). Phosphorylation of the polymeric immunoglobulin receptor required for its efficient transcytosis. Science *248*, 742–745.

Castro-Alamancos, M.A., and Calcagnotto, M.E. (1999). Presynaptic long-term potentiation in corticothalamic synapses. J. Neurosci. *19*, 9090–9097.

Chen, C., and Regehr, W.G. (2000). Developmental remodeling of the retinogeniculate synapse. Neuron *28*, 955–966.

Dingledine, R., Borges, K., Bowie, D., and Traynelis, S.F. (1999). The glutamate receptor ion channels. Pharmacol. Rev. *51*, 7–61.

Ehlers, M.D. (2000). Reinsertion or degradation of AMPA receptors determined by activity-dependent endocytic sorting. Neuron *28*, 511–525.

Ehlers, M.D., Heine, M., Groc, L., Lee, M.C., and Choquet, D. (2007). Diffusional trapping of GluR1 AMPA receptors by input-specific synaptic activity. Neuron *54*, 447–460.

English, J.D., and Sweatt, J.D. (1997). A requirement for the mitogen-activated protein kinase cascade in hippocampal long term potentiation. J. Biol. Chem. *272*, 19103–19106.

Erisir, A., and Harris, J.L. (2003). Decline of the critical period of visual plasticity is concurrent with the reduction of NR2B subunit of the synaptic NMDA receptor in layer 4. J. Neurosci. *23*, 5208–5218.

Erisir, A., Van Horn, S.C., and Sherman, S.M. (1997). Relative numbers of cortical and brainstem inputs to the lateral geniculate nucleus. Proc. Natl. Acad. Sci. USA *94*, 1517–1520.

Esteban, J.A., Shi, S.H., Wilson, C., Nuriya, M., Huganir, R.L., and Malinow, R. (2003). PKA phosphorylation of AMPA receptor subunits controls synaptic trafficking underlying plasticity. Nat. Neurosci. *6*, 136–143.

Fremeau, R.T., Jr., Troyer, M.D., Pahner, I., Nygaard, G.O., Tran, C.H., Reimer, R.J., Bellocchio, E.E., Fortin, D., Storm-Mathisen, J., and Edwards, R.H. (2001). The expression of vesicular glutamate transporters defines two classes of excitatory synapse. Neuron *31*, 247–260.

Friedman, H.V., Bresler, T., Garner, C.C., and Ziv, N.E. (2000). Assembly of new individual excitatory synapses: time course and temporal order of synaptic molecule recruitment. Neuron *27*, 57–69.

Fu, Z., Lee, S.H., Simonetta, A., Hansen, J., Sheng, M., and Pak, D.T. (2007). Differential roles of Rap1 and Rap2 small GTPases in neurite retraction and synapse elimination in hippocampal spiny neurons. J. Neurochem. *100*, 118–131.

Gao, C., Sun, X., and Wolf, M.E. (2006). Activation of D1 dopamine receptors increases surface expression of AMPA receptors and facilitates their synaptic incorporation in cultured hippocampal neurons. J. Neurochem. *98*, 1664–1677.

Gardner, S.M., Trussell, L.O., and Oertel, D. (2001). Correlation of AMPA receptor subunit composition with synaptic input in the mammalian cochlear nuclei. J. Neurosci. *21*, 7428–7437.

Geiger, J.R., Lubke, J., Roth, A., Frotscher, M., and Jonas, P. (1997). Submillisecond AMPA receptor-mediated signaling at a principal neuron-interneuron synapse. Neuron *18*, 1009–1023.

Gu, Y., and Stornetta, R.L. (2007). Synaptic plasticity, AMPA-R trafficking, and Ras-MAPK signaling. Acta Pharmacol. Sin. *28*, 928–936.

Guido, W. (2008). Refinement of the retinogeniculate pathway. J. Physiol. *586*, 4357–4362.

Hammerton, R.W., Krzeminski, K.A., Mays, R.W., Ryan, T.A., Wollner, D.A., and Nelson, W.J. (1991). Mechanism for regulating cell surface distribution of Na+,K(+)-ATPase in polarized epithelial cells. Science *254*, 847–850.

Hausser, M., and Roth, A. (1997). Estimating the time course of the excitatory synaptic conductance in neocortical pyramidal cells using a novel voltage jump method. J. Neurosci. *17*, 7606–7625.

Hayashi, Y., Shi, S.H., Esteban, J.A., Piccini, A., Poncer, J.C., and Malinow, R. (2000). Driving AMPA receptors into synapses by LTP and CaMKII: requirement for GluR1 and PDZ domain interaction. Science *287*, 2262–2267.

Hettinger, B.D., Lee, A., Linden, J., and Rosin, D.L. (2001). Ultrastructural localization of adenosine A2A receptors suggests multiple cellular sites for modulation of GABAergic neurons in rat striatum. J. Comp. Neurol. *431*, 331–346.

Hoffman, D.A., Magee, J.C., Colbert, C.M., and Johnston, D. (1997). K+ channel regulation of signal propagation in dendrites of hippocampal pyramidal neurons. Nature *387*, 869–875.

Hooks, B.M., and Chen, C. (2006). Distinct roles for spontaneous and visual activity in remodeling of the retinogeniculate synapse. Neuron *52*, 281–291.

Hsieh, H., Boehm, J., Sato, C., Iwatsubo, T., Tomita, T., Sisodia, S., and Malinow, R. (2006). AMPAR removal underlies Abeta-induced synaptic depression and dendritic spine loss. Neuron *52*, 831–843.

Hu, H., Qin, Y., Bochorishvili, G., Zhu, Y., van Aelst, L., and Zhu, J.J. (2008). Ras signaling mechanisms underlying impaired GluR1-dependent plasticity associated with fragile X syndrome. J. Neurosci. *28*, 7847–7862.

Huang, Z.J., and Scheiffele, P. (2008). GABA and neuroligin signaling: linking synaptic activity and adhesion in inhibitory synapse development. Curr. Opin. Neurobiol. *18*, 77–83.

Impey, S., Obrietan, K., Wong, S.T., Poser, S., Yano, S., Wayman, G., Deloulme, J.C., Chan, G., and Storm, D.R. (1998). Cross talk between ERK and PKA is required for Ca2+ stimulation of CREB-dependent transcription and ERK nuclear translocation. Neuron *21*, 869–883.

Isaac, J.T., Ashby, M., and McBain, C.J. (2007). The role of the GluR2 subunit in AMPA receptor function and synaptic plasticity. Neuron *54*, 859–871.

Jonas, P. (2000). The time course of signaling at central glutamatergic synapses. News Physiol. Sci. *15*, 83–89.

Kessels, H.W., and Malinow, R. (2009). Synaptic AMPA receptor plasticity and behavior. Neuron *61*, 340–350.

Kielland, A., Erisir, A., Walaas, S.I., and Heggelund, P. (2006). Synapsin utilization differs among functional classes of synapses on thalamocortical cells. J. Neurosci. *26*, 5786–5793.

Kolleker, A., Zhu, J.J., Schupp, B.J., Qin, Y., Mack, V., Borchardt, T., Kohr, G., Malinow, R., Seeburg, P.H., and Osten, P. (2003). Glutamatergic plasticity by synaptic delivery of GluR-B(long)-containing AMPA receptors. Neuron *40*, 1199–1212.

Lai, H.C., and Jan, L.Y. (2006). The distribution and targeting of neuronal voltage-gated ion channels. Nat. Rev. Neurosci. *7*, 548–562.

Liebmann, C. (2001). Regulation of MAP kinase activity by peptide receptor signalling pathway: paradigms of multiplicity. Cell. Signal. *13*, 777–785.

Liu, X., and Chen, C. (2008). Different roles for AMPA and NMDA receptors in transmission at the immature retinogeniculate synapse. J. Neurophysiol. *99*, 629–643.

Luttrell, L.M. (2003). 'Location, location, location': activation and targeting of MAP kinases by G protein-coupled receptors. J. Mol. Endocrinol. *30*, 117–126.

Malenka, R.C., Kauer, J.A., Perkel, D.J., Mauk, M.D., Kelly, P.T., Nicoll, R.A., and Waxham, M.N. (1989). An essential role for postsynaptic calmodulin and protein kinase activity in long-term potentiation. Nature *340*, 554–557.

Malinow, R., Schulman, H., and Tsien, R.W. (1989). Inhibition of postsynaptic PKC or CaMKII blocks induction but not expression of LTP. Science *245*, 862–866.

Martin, L.J., Blackstone, C.D., Levey, A.I., Huganir, R.L., and Price, D.L. (1993). AMPA glutamate receptor subunits are differentially distributed in rat brain. Neuroscience *53*, 327–358.

Matsuda, S., Miura, E., Matsuda, K., Kakegawa, W., Kohda, K., Watanabe, M., and Yuzaki, M. (2008). Accumulation of AMPA receptors in autophagosomes in neuronal axons lacking adaptor protein AP-4. Neuron *57*, 730–745.

McAllister, A.K. (2007). Dynamic aspects of CNS synapse formation. Annu. Rev. Neurosci. *30*, 425–450.

McCormack, S.G., Stornetta, R.L., and Zhu, J.J. (2006). Synaptic AMPA receptor exchange maintains bidirectional plasticity. Neuron *50*, 75–88.

Mellman, I., and Nelson, W.J. (2008). Coordinated protein sorting, targeting and distribution in polarized cells. Nat. Rev. Mol. Cell Biol. *9*, 833–845.

Mineff, E.M., and Weinberg, R.J. (2000). Differential synaptic distribution of AMPA receptor subunits in the ventral posterior and reticular thalamic nuclei of the rat. Neuroscience *101*, 969–982.

Mosbacher, J., Schoepfer, R., Monyer, H., Burnashev, N., Seeburg, P.H., and Ruppersberg, J.P. (1994). A molecular determinant for submillisecond desensitization in glutamate receptors. Science *266*, 1059–1062.

Nonaka, H., Takei, K., Umikawa, M., Oshiro, M., Kuninaka, K., Bayarjargal, M., Asato, T., Yamashiro, Y., Uechi, Y., Endo, S., et al. (2008). MINK is a Rap2 effector for phosphorylation of the postsynaptic scaffold protein TANC1. Biochem. Biophys. Res. Commun. *377*, 573–578.

Oh, M.C., Derkach, V.A., Guire, E.S., and Soderling, T.R. (2006). Extrasynaptic membrane trafficking regulated by GluR1 serine 845 phosphorylation primes AMPA receptors for long-term potentiation. J. Biol. Chem. *281*, 752–758.

Okamoto, K., Narayanan, R., Lee, S.H., Murata, K., and Hayashi, Y. (2007). The role of CaMKII as an F-actin-bundling protein crucial for maintenance of dendritic spine structure. Proc. Natl. Acad. Sci. USA *104*, 6418–6423.

Park, M., Penick, E.C., Edwards, J.G., Kauer, J.A., and Ehlers, M.D. (2004). Recycling endosomes supply AMPA receptors for LTP. Science *305*, 1972–1975.

Park, M., Salgado, J.M., Ostroff, L., Helton, T.D., Robinson, C.G., Harris, K.M., and Ehlers, M.D. (2006). Plasticity-induced growth of dendritic spines by exocytic trafficking from recycling endosomes. Neuron *52*, 817–830.

Pelkey, K.A., Topolnik, L., Lacaille, J.C., and McBain, C.J. (2006). Compartmentalized Ca(2+) channel regulation at divergent mossy-fiber release sites underlies target cell-dependent plasticity. Neuron *52*, 497–510.

Perreault, M.C., Qin, Y., Heggelund, P., and Zhu, J.J. (2003). Postnatal development of GABAergic signalling in the rat lateral geniculate nucleus: presynaptic dendritic mechanisms. J. Physiol. *546*, 137–148.

Petralia, R.S., and Wenthold, R.J. (1992). Light and electron immunocytochemical localization of AMPA-selective glutamate receptors in the rat brain. J. Comp. Neurol. *318*, 329–354.

Qin, Y., Zhu, Y., Baumgart, J.P., Stornetta, R.L., Seidenman, K., Mack, V., van Aelst, L., and Zhu, J.J. (2005). State-dependent Ras signaling and AMPA receptor trafficking. Genes Dev. *19*, 2000–2015.

Rizzoli, S.O., and Betz, W.J. (2005). Synaptic vesicle pools. Nat. Rev. Neurosci. *6*, 57–69.

Roberson, E.D., English, J.D., Adams, J.P., Selcher, J.C., Kondratick, C., and Sweatt, J.D. (1999). The mitogen-activated protein kinase cascade couples PKA and PKC to cAMP response element binding protein phosphorylation in area CA1 of hippocampus. J. Neurosci. *19*, 4337–4348.

Rubio, M.E., and Wenthold, R.J. (1997). Glutamate receptors are selectively targeted to postsynaptic sites in neurons. Neuron *18*, 939–950.

Sampo, B., Kaech, S., Kunz, S., and Banker, G. (2003). Two distinct mechanisms target membrane proteins to the axonal surface. Neuron *37*, 611–624.

Schaefer, A.T., Helmstaedter, M., Schmitt, A.C., Bar-Yehuda, D., Almog, M., Ben-Porat, H., Sakmann, B., and Korngreen, A. (2007). Dendritic voltage-gated K+ conductance gradient in pyramidal neurones of neocortical layer 5B from rats. J. Physiol. *579*, 737–752.

Schuck, S., and Simons, K. (2004). Polarized sorting in epithelial cells: raft clustering and the biogenesis of the apical membrane. J. Cell Sci. *117*, 5955–5964.

Serulle, Y., Zhang, S., Ninan, I., Puzzo, D., McCarthy, M., Khatri, L., Arancio, O., and Ziff, E.B. (2007). A GluR1-cGKII interaction regulates AMPA receptor trafficking. Neuron *56*, 670–688.

Setou, M., Nakagawa, T., Seog, D.H., and Hirokawa, N. (2000). Kinesin superfamily motor protein KIF17 and mLin-10 in NMDA receptor-containing vesicle transport. Science *288*, 1796–1802.

Shepherd, J.D., and Huganir, R.L. (2007). The cell biology of synaptic plasticity: AMPA receptor trafficking. Annu. Rev. Cell Dev. Biol. *23*, 613–643.

Sherman, S.M., and Guillery, R.W. (2002). The role of the thalamus in the flow of information to the cortex. Philos. Trans. R. Soc. Lond. B Biol. Sci. *357*, 1695–1708.

Silva, A.J., Stevens, C.F., Tonegawa, S., and Wang, Y. (1992). Deficient hippocampal long-term potentiation in alpha-calcium- calmodulin kinase II mutant mice. Science *257*, 201–206.

Smith, F.D., Langeberg, L.K., and Scott, J.D. (2006). The where's and when's of kinase anchoring. Trends Biochem. Sci. *31*, 316–323.

Steinberg, S.F. (2008). Structural basis of protein kinase C isoform function. Physiol. Rev. *88*, 1341–1378.

Steiner, P., Higley, M.J., Xu, W., Czervionke, B.L., Malenka, R.C., and Sabatini, B.L. (2008). Destabilization of the postsynaptic density by PSD-95 serine 73 phosphorylation inhibits spine growth and synaptic plasticity. Neuron *60*, 788–802.

Steriade, M., Jones, E.G., and McCormick, D. (1997). Thalamus (Amsterdam, New York: Elsevier).

Tada, T., and Sheng, M. (2006). Molecular mechanisms of dendritic spine morphogenesis. Curr. Opin. Neurobiol. *16*, 95–101.

Takahashi, T., Svoboda, K., and Malinow, R. (2003). Experience strengthening transmission by driving AMPA receptors into synapses. Science *299*, 1585–1588.

Tasken, K., and Aandahl, E.M. (2004). Localized effects of cAMP mediated by distinct routes of protein kinase A. Physiol. Rev. *84*, 137–167.

Toth, K., and McBain, C.J. (1998). Afferent-specific innervation of two distinct AMPA receptor subtypes on single hippocampal interneurons. Nat. Neurosci. *1*, 572–578.

Turner, J.P., and Salt, T.E. (1998). Characterization of sensory and corticothalamic excitatory inputs to rat thalamocortical neurones in vitro. J. Physiol. *510*, 829–843.

Usrey, W.M., Reppas, J.B., and Reid, R.C. (1998). Paired-spike interactions and synaptic efficacy of retinal inputs to the thalamus. Nature *395*, 384–387.

Vacher, H., Mohapatra, D.P., and Trimmer, J.S. (2008). Localization and targeting of voltage-dependent ion channels in Mammalian central neurons. Physiol. Rev. *88*, 1407–1447.

Walker, H.C., Lawrence, J.J., and McBain, C.J. (2002). Activation of kinetically distinct synaptic conductances on inhibitory interneurons by electrotonically overlapping afferents. Neuron *35*, 161–171.

Wang, W., Jones, H.E., Andolina, I.M., Salt, T.E., and Sillito, A.M. (2006). Functional alignment of feedback effects from visual cortex to thalamus. Nat. Neurosci. *9*, 1330–1336.

Washbourne, P., Liu, X.B., Jones, E.G., and McAllister, A.K. (2004). Cycling of NMDA receptors during trafficking in neurons before synapse formation. J. Neurosci. *24*, 8253–8264.

Yang, Y., Wang, X.B., Frerking, M., and Zhou, Q. (2008). Delivery of AMPA receptors to perisynaptic sites precedes the full expression of long-term potentiation. Proc. Natl. Acad. Sci. USA *105*, 11388–11393.

Yap, C.C., Wisco, D., Kujala, P., Lasiecka, Z.M., Cannon, J.T., Chang, M.C., Hirling, H., Klumperman, J., and Winckler, B. (2008). The somatodendritic endosomal regulator NEEP21 facilitates axonal targeting of L1/NgCAM. J. Cell Biol. *180*, 827–842.

Yasuda, R., Harvey, C.D., Zhong, H., Sobczyk, A., van Aelst, L., and Svoboda, K. (2006). Supersensitive Ras activation in dendrites and spines revealed by two-photon fluorescence lifetime imaging. Nat. Neurosci. *9*, 283–291.

Zhu, J.J. (2000). Maturation of layer 5 neocortical pyramidal neurons: amplifying salient layer 1 and layer 4 inputs by Ca2+ action potentials in adult rat tuft dendrites. J. Physiol. *526*, 571–587.

Zhu, J.J., Esteban, J.A., Hayashi, Y., and Malinow, R. (2000). Postnatal synaptic potentiation: delivery of GluR4-containing AMPA receptors by spontaneous activity. Nat. Neurosci. *3*, 1098–1106.

Zhu, J.J., Qin, Y., Zhao, M., Van Aelst, L., and Malinow, R. (2002). Ras and Rap control AMPA receptor trafficking during synaptic plasticity. Cell *110*, 443–455.

Zhu, Y., Pak, D., Qin, Y., McCormack, S.G., Kim, M.J., Baumgart, J.P., Velamoor, V., Auberson, Y.P., Osten, P., van Aelst, L., et al. (2005). Rap2-JNK removes synaptic AMPA receptors during depotentiation. Neuron *46*, 905–916.

Zucker, R.S., and Regehr, W.G. (2002). Short-term synaptic plasticity. Annu. Rev. Physiol. *64*, 355–405.